Drone-based meteorological observations up to the tropopause

Konrad Bärfuss[1], Holger Schmithüsen[2], and Astrid Lampert[1]

[1]Technische Universität Braunschweig, Institute of Flight Guidance, 38108 Braunschweig, Germany
[2]Alfred Wegener Institute, Helmholtz Centre for Polar and Marine Research, 27570 Bremerhaven, Germany

Correspondence: Konrad Bärfuss (k.baerfuss@tu-braunschweig.de)

Abstract. The main in-situ data base for numerical weather prediction currently relies on radiosonde and airliner observations, with large data gaps in the atmospheric boundary layer, above the oceans and in polar regions. These gaps might possibly be patched by measurements with drones, which provide a significant improvement towards environment friendly additional data, but so far have not been regarded as a feasible alternative of performing measurements in the upper troposphere. In this report, the development of a system that is capable of sounding the atmosphere under Antarctic and mid-European conditions is presented. After an assessment of the environmental conditions, the design of the system and the measurements are presented, including the process to get permissions for such flight tests in Europe. The feasibility of reaching an altitude of 10 km with a small meteorologically equipped drone is shown, and the first data are compared to radiosonde measurements demonstrating accuracy comparable to other aircraft based observations, despite the simplistic sensor package deployed. The article closes with an outlook on the potential use of drones for filling data gaps in the troposphere.

1 Introduction

Accurate weather predictions are of high importance for humankind, from agriculture via air traffic, warning of severe weather events like storm and heavy rain to the personal activities of individuals. With increasing computational power, there have been significant improvements in operational weather models (Bauer et al., 2015). However, these global and mesoscale models require measurement data as input to tie the short-term forecast towards observations (Wang et al., 2000). In this computing-intensive process, data can be assimilated continuously, with high flexibility regarding spatial and temporal resolution and trajectory (Bonavita et al., 2016). The data to be assimilated originates from the World Meteorological Organisation (WMO) Global Observing System (Thépaut and Andersson, 2010; WMO, 2010, 2015a), consisting of measurements using both in-situ and remote sensing techniques. Atmospheric measurements of pressure, temperature, humidity, wind speed and wind direction are crucial to Numerical Weather Prediction (NWP). These measurements can partially be provided by ground based remote sensing techniques (Lindskog et al., 2004; Kotthaus et al., 2022), satellite based remote sensing techniques (Steiner et al., 2001; Karbou et al., 2005; Rennie et al., 2021), radiosondes (Ingleby et al., 2016a), aircraft (Fleming, 1996) and dropsondes (meteorological sensor packets dropped from high altitude platforms (Hock and Franklin, 1999). Each of these observing system types has its own peculiarities which have to be considered for implementing in weather models, and has a different impact on the forecast quality.

Ground based remote sensing instruments need significant financial effort to be deployed and operated. Their use around the

globe is therefore quite limited. Satellite based remote sensing measurements provide superior global coverage and have a high impact in NWP (Cardinali, 2009), especially over data-poor areas (Bouttier and Kelly, 2001). For calibration and validation of these satellite sensors and data products, satellite based observing systems (and in general remote sensing measurements) rely on in-situ data for calibration and validation (Goldberg et al., 2011; Chander et al., 2013; Boylan et al., 2015; Carminati et al., 2019). An increasing challenge (and also a potential opportunity, Palmer et al., 2021) for retrieving meteorological observations from satellite microwave instruments (e.g. Karbou et al., 2005) is the "society's insatiable need for the radio spectrum." (Palmer et al., 2021), potentially harming future measurements. Space-based Doppler Wind Lidar measurements are regarded as essential data for weather models, addressing the urgent need in providing wind profiles at all latitudes and altitudes (Baker et al., 2014).

Of major importance regarding in-situ observations are vertical profiles measured by radiosondes. They are launched at specific stations and at fixed launch times, from typically daily to 4 times per day. The measurement data are transferred to the ground via telemetry, and are sent to the network Global Telecommunication System (GTS) to be accessed by weather services in a specific data format (Ingleby and Edwards, 2015). Typical state of the art sounding systems provide measurements of altitude, pressure, temperature, humidity, wind speed and wind direction once per second. Depending on the sounding system and balloon sizes used, radiosondes typically measure atmospheric profiles up to an altitude of 35 km or even 40 km, covering the entire troposphere and most of the stratosphere. Usually, radiosondes are not collected and re-used, but remain in the landscape as litter. The worldwide around 800 radiosonde launch sites are not evenly distributed around the globe. There are large areas with only few regular launches, in particular above the oceans and in the polar regions.

Another important source of in-situ data originates from the AMDAR (Aircraft Meteorological DAta Relay) and the U.S. related TAMDAR (Tropospheric Airborne Meteorological Data Reporting) programme (Moninger et al., 2003; Petersen et al., 2015, 2016; Petersen, 2016). In the vicinity of large cities, vertical profiles of temperature, wind speed and wind direction (and partly humidity) are measured frequently through commercial aircraft equipped with the AMDAR specific meteorological sensor package (WMO, 2003), whereas data from level flight is acquired on main aircraft routes. For this airborne method, a careful calibration and processing of the data is required (de Haan et al., 2022). Due to less coverage with enroute flights and especially airports, regions like the Arctic and Antarctic as well as mid-Africa suffer from a lower data density regarding the AMDAR system.

Data comparable to aircraft and radiosonde measurements can be gathered using sondes dropped by aircraft - either crewed (Laursen et al., 2006) or uncrewed (Kren et al., 2018) - and balloons (Wang et al., 2013) from altitudes close to the ground up to 30 km (Cohn et al., 2013). Data from dropsonde measurements have recently been used for intense observation periods (Redelsperger et al., 2006; Rabier et al., 2010; Kren et al., 2018; Schindler et al., 2020; Ralph et al., 2020; Zheng et al., 2021)~~but caused by their targeted use~~, but as they are used for specific target areas and specific purposes only, they do not play a significant role in global observations.

To assess the impact on forecast quality and subsequently the importance of these different observing systems (single observation systems) in order to further develop the Global Observing System, Observation System Experiments (Bormann et al., 2019), Sensitivity to Observation (Cardinali, 2013; Langland and Baker, 2004) and similar experiments (Ingleby et al., 2020;

Ota et al., 2013) can be carried out. As new observing systems are deployed, their impact on weather models (including the assimilation system) is evaluated and reviewed using these techniques ~~(Rennie et al., 2021; Petersen, 2016; Petersen et al., 2016; Bouttier and~~ (Rennie et al., 2021; Petersen, 2016; Petersen et al., 2016; Bouttier and Kelly, 2001; Bormann et al., 2019; Riishojgaard, 2015) . For example space-based Doppler Wind Lidar measurements are regarded as essential for numerical weather prediction (Baker et al., 2014). The examination of including wind retrievals using the first space-borne wind ~~lidar (Rennie et al., 2021),~~ Lidar showed a positive impact on forecasting quality (Rennie et al., 2021). Aircraft meteorological measurements complement radiosonde measurements when radiosonde data was not used in the forecast experiments (Gelaro and Zhu, 2009; Lorenc and Marriott, 2014; Kim and Kim, 2019). Aircraft wind and temperature reports show a significant improvement of model results at pressure levels between 700 - 400 hPa (around 3-7 km altitude) (Petersen, 2016). ~~Aircraft~~ The availability of additional aircraft humidity data have the highest impact between 1000 - 400 hPa (around 0.5-7 km altitude) (Petersen et al., 2016), whereas additional radiosonde in-situ humidity data has the highest influence on weather models at 700 - 600 hPa (around 3-4 km altitude) (Ota et al., 2013). In comparison with temperature and wind, the impact of aircraft humidity data showed lower influence on the results of weather models (Ingleby et al., 2020).

Summing up the components of the Global Observation System, in-situ data gaps of important observations are obvious, as radiosonde and aircraft based soundings are sparsely distributed over remote areas and oceans, associated with increased impact of additional radiosonde observations (Ota et al., 2013). The density of observations is not well balanced with the user requirements for observations. Breakthrough requirements from data users exceed today's capabilities of the Global Observation System in terms of temporal and spatial resolution for the use case of global and high resolution numerical weather prediction. These requirements differ between their application area and the variable, e.g. for global NWP, the breakthrough requirement for the spatial resolution of temperature measurements is 100 km horizontally and 1 km vertically (Leuenberger et al., 2020). Generally spoken, more and higher resolution data lead to improved numerical simulations of both local and regional weather forecast (Faccani et al., 2009). Numerical weather prediction models perform best with observations of similar temporal and spatial resolution as in the model (Dabberdt et al., 2005).

Besides regional data gaps (Ingleby et al., 2016b; WMO, 2020) and general data gaps (Houston et al., 2021), there is a data gap in the lower troposphere in atmospheric observing systems (Leuenberger et al., 2020; Pinto et al., 2021), and the potential of ~~Uncrewed (Joyce et al., 2021) Aerial Systems (UAS)~~ drones to fill the gap is currently being discussed. ~~UAS~~ Drones (also called ~~drones~~unmanned or uncrewed (Joyce et al., 2021) aircraft systems, remotely piloted aircraft systems, RPAS) provide a flexible tool for atmospheric sensing. The use of small ~~UAS~~ drones as a platform for meteorological sensors dates back to the early 1960's (Konrad et al., 1970). Far from being mature back in the 60ies, their use was limited to augmented line of sight operations using binoculars and therefore the use in the lower troposphere. A comprehensive review of the historical and recent use of ~~fixed wing uncrewed aircraft~~ fixed-wing drones for meteorological sensing can be found in Elston et al. (2015). In consequence of the emergence of commercial off-the-shelf ~~UAS~~ drones (both fixed-wing and multicopter), the use of ~~UAS~~ drones in different fields of research rapidly increased during the last decade.

The atmospheric boundary layer experiences high temporal changes, and as being closely connected to the spatially variable Earth surface, the boundary layer plays a key role in initiating or hindering weather events like convection or cloud and fog

formation. Therefore ~~UAS~~ drone measurements in the boundary layer have a high potential for providing data of added value to weather forecast (Inoue and Sato, 2022), for example by determining the boundary layer altitude capped by a temperature inversion (Jonassen et al., 2012; Flagg et al., 2018).

The improvement of assimilating ~~UAS~~ drone measurements of the atmospheric boundary layer in numerical weather predictions during intensive meteorological campaigns has been demonstrated (de Boer et al., 2020), with improvements of modelling results for a distance up to 300 km (Sun et al., 2020). Significant benefit from regular ~~UAS~~ drone soundings even to limited altitudes of 1 km or 3 km has been demonstrated for precipitation (Chilson et al., 2019) and cloud coverage (Leuenberger et al., 2020), and a reduction of over 40 % for the root mean square error and bias in the 15 min forecasts of temperature, wind and humidity between the benchmark run and a model run with assimilated data of a coordinated fleet of ~~UAS was observed (Jensen et al., 2021)~~drones was observed (Jensen et al., 2021, 2022), despite the challenges of data assimilation in mountainous environments (Hacker et al., 2018). However, ~~UAS~~ drone measurements up to higher altitudes would be more beneficial (Sun et al., 2020).

For obtaining additional data similar to the classical radiosondes, balloon-launched ~~UAS~~ drones which are carried up to a certain altitude, which can be around 20-40 km, have been developed. Once reaching the target altitude, the systems are released from the balloons and then return to the starting location in restricted air space ~~(Kräuchi and Philipona, 2016; Schuyler et al., 2019; Lafon et~~ (Lafon et al., 2014; Kräuchi and Philipona, 2016; Schuyler et al., 2019) - at least for low wind speed conditions. These ~~UAS~~ drones further provide the advantage of controlling the direction of flight. In comparison to radiosondes, it is therefore possible to deploy more sophisticated instrumentation, as it can be used multiple times, and sensors can be calibrated before and after a sounding for quality checks. High data quality enables further use of the measurements such as climate applications ~~(see ANNEX 12.B in WMO (2018))~~(see ANNEX 12.B in WMO, 2018). However, balloon launched systems require the availability of helium and a certain launching infrastructure, like for the classical radiosonde launches, and are barely able to glide back to their starting location for wind speed exceeding 15 $\mathrm{m\,s^{-1}}$.

For increasing the flexibility of the launching site, it is beneficial to deploy systems with own propulsion. Regular soundings of multicopter ~~UAS~~ drones to improve weather forecast for airports have been established in Switzerland (Leuenberger et al., 2020). Other studies to improve weather prediction include fixed-wing ~~UAS~~ drones as well (Koch et al., 2018). Further, no waste is left from such ~~an UAS~~ a drone ascent, which is of high importance in particular in the Antarctic, where the Antarctic Treaty requires Environmental Impact Assessments to be developed for all activities and which sets rules for waste disposal and management (Secretariat of the Antarctic Treaty, 2019). Nevertheless, systems with own propulsion normally do not reach the altitudes of radiosondes, and therefore can be compared more easily to aircraft (e.g. AMDAR/TAMDAR). The main technical challenges of ~~UAS~~ drone operations up to high altitudes comparable ~~to aircraft based~~ observations on commercial aircraft are high wind speed, low temperatures and potential icing. Individual systems and concepts have been developed for applications in high wind speed, like for in-situ measurements of hurricanes and tornadic supercells (Cione et al., 2020; Elston et al., 2011) and for measurements up to and within the stratosphere (Runge et al., 2007).

Nowadays, the status of small ~~uncrewed aerial systems~~ drones for weather sensing in the lower troposphere is quite mature (Pinto et al., 2021) and close to being ready for operational applications in meteorology. As an experiment to collect experi-

ence on both the ~~UAS~~ drone operation as well as the NWP side, the WMO is preparing a worldwide coordinated demonstration campaign in 2024 (WMO, 2022). There is broad agreement that ~~UAS~~ drones are becoming an increasingly important tool for all sorts of meteorological tasks ~~(Geerts et al., 2018; Vömel et al., 2018)~~(Geerts et al., 2018; Vömel et al., 2018). Interestingly, ~~UAS~~ drones which are capable of reaching the upper troposphere and even lower stratosphere are viewed to play an important role and enable the community to address important scientific issues, but these systems did not receive much attention in the science discussion - the road to inexpensive high flying ~~UAS~~ drones seemed to remain unpaved.

The importance of aircraft measurements in the troposphere concomitant with in-situ data gaps in the troposphere and over remote areas was the starting point for a research project at the Technische Universität Braunschweig (Germany), in which a ~~UAS~~ drone was developed to augment in-situ data in Antarctica. The ~~UAS~~ drone represents a fairly unusual class ~~(medium altitude, short endurance, Watts et al. (2012))~~(medium altitude, short endurance, Watts et al., 2012). The propelled ~~UAS~~ drone technique presented here provides the capability of sounding the entire troposphere vertically or perform level legs at designated altitudes while measuring pressure, temperature, humidity, wind speed, wind direction and turbulence, and flexibly addressing the data needs (Houston et al., 2021). Regarding data assimilation, ~~UAS~~ drone data transferred to the GTS is similar to aircraft data (especially true for regional aircraft observations, Moninger et al., 2010) and radiosonde data (ascent and descent).

This feasibility study presents the concept, design and first applications of the system *LUCA* (Lightweight Unmanned high Ceiling Aerial system), which was developed to provide complementary in-situ data up to an altitude of 10 km at flexible locations. Simultaneous radiosonde ascents are used to validate the quality of the meteorological observations acquired during the first flights.

2 Methods

In the following, the process towards the design of the ~~UAS~~ drone of type *LUCA* is presented briefly. Requirements for the system concern data quality on the one hand, and dealing with the harsh environmental conditions and availability of measurements on the other hand. The environmental conditions for operations of the ~~UAS~~ drone are described. Based on this, the design of the mission and of the ~~UAS~~ drone is introduced. The ~~sensor package~~ simplistic sensor package used is described, including datasheet measurement uncertainties. ~~Finally~~Before introducing to postprocessing calculi and methods to assess the data quality, the process of flight permissions is presented.

The section closes with a note on the variability of the atmosphere.

2.1 Environmental conditions

LUCA was designed to operate in mid-latitude and polar conditions. Therefore, the expected environmental constraints were evaluated from the radiosonde stations Neumayer in Antarctica and Lindenberg in Germany (Figure 1) for a time period of three years (2016-2018). The temperature range covering 90% of the operation conditions of the ascents at Lindenberg is be-

tween -60°C and 20°C and at Neumayer between -75°C and -2°C. For the station Lindenberg, the median wind speed is up to 20 m s^{-1} (39 ~~kts~~kn), and the wind speed that is encountered in 90% of the cases (90% percentile) is up to 42 m s^{-1} (81 ~~kts~~kn) for the altitude of the jet stream (7-15 km) (Pena-Ortiz et al., 2013). For the station Neumayer, the median wind speed is up to 14 m s^{-1} (27 ~~kts), but~~ kn), and the wind speed that can be expected in 90% of the cases is up to 28 m s^{-1} (54 ~~kts~~kn).

Operational challenges at Neumayer arise from the surface wind speed, which is generally higher than in Europe. The most frequent surface wind conditions are either from East due to cyclonic activities near the polar front, with typical wind speed of 20 m s^{-1} (39 ~~kts~~kn), or from S due to katabatic flow, with typical wind speed of 10 m s^{-1} (19 ~~kts~~kn) (König-Langlo et al., 1998). High wind speed values are further reached at the altitude of the tropopause around 9-13 km (Evtushevsky et al., 2008) in the polar jet stream (Archer and Caldeira, 2008).

As a trade-off for *LUCA*, the system was designed for operation in the temperature range between -75°C and +30°C and for ~~a wind speed~~ an integral mean wind speed over the whole vertical profile of up to 28 m s^{-1} (54 ~~kts~~kn). Assuming the system is capable of operating in conditions exceeding the design temperature and nominal wind speed with 15 %, this would allow ascents in 87 % of the radiosonde days at Neumayer in the Antarctic and 72 % at Lindenberg. Applying an integral wind speed condition such that the drone does not have to stay above the launch point, but must be able to return to the base, the mean wind speed over the atmospheric profile to be observed by the drone should not exceed the nominal airspeed. despite the limited applicability of this approach when using the drone in a reserved airspace and ignoring possible environmental threats such as heavy precipitation or inflight icing, the system is capable of covering 94 % of the measurements in Lindenberg and 98 % at the Neumayer station. Adding the margin of 15 %, the availability increases to 97 % for Lindenberg, and 100 % at Neumayer. At Neumayer Station, typically on 96% of the days radiosondes can be launched. Lindenberg has a temporal coverage of 99% of all days. In addition, the development of the ~~UAS~~ drone addresses measurements during rainfall, snow, heavy turbulence and within clouds.

Particular attention was payed to takeoff and landing under high surface wind conditions, which are accompanied at the Neumayer Station by low visibility due to drifting and blowing snow. The probability of 23 % to operate under conditions with a visibility below 500 m requires a highly automated take-off and landing procedure, which does not rely on visual contact of the operator with the system, similar to operations shown by Reineman et al. (2016).

A possible threat for ~~UAS~~ drone measurements are inflight icing conditions, which depend on temperature, humidity and droplet size (Jeck, 2002). An idea of the frequency of icing conditions might be available of icing forecast data using ADWICE (Advanced Diagnosis and Warning system for aircraft Icing Environments, Tafferner et al., 2003) along with validation studies using PIREPs (PIlot REPorts). Such comparisons exist for regions with dense air traffic, e.g. Europe (Kalinka et al., 2017), but no validation studies are found for the Antarctic. In addition, icing differs strongly between manned aircraft (what ADWICE is made for) and ~~UAS~~ drones (Hann, 2020). A report for Norway and surrounding regions explicitly focused on icing for ~~UAS~~ drones using meteorological reanalysis data (ECMWF ERA5, Hersbach et al., 2020) and an ice accretion model (ICE3D, Sørensen et al., 2021), and found icing frequencies of 45 % at an altitude between 1 km - 1.5 km between September and May, and a lower risk with the highest frequency of 30 % peaking at 2.5 km altitude in June to August. These values are not directly

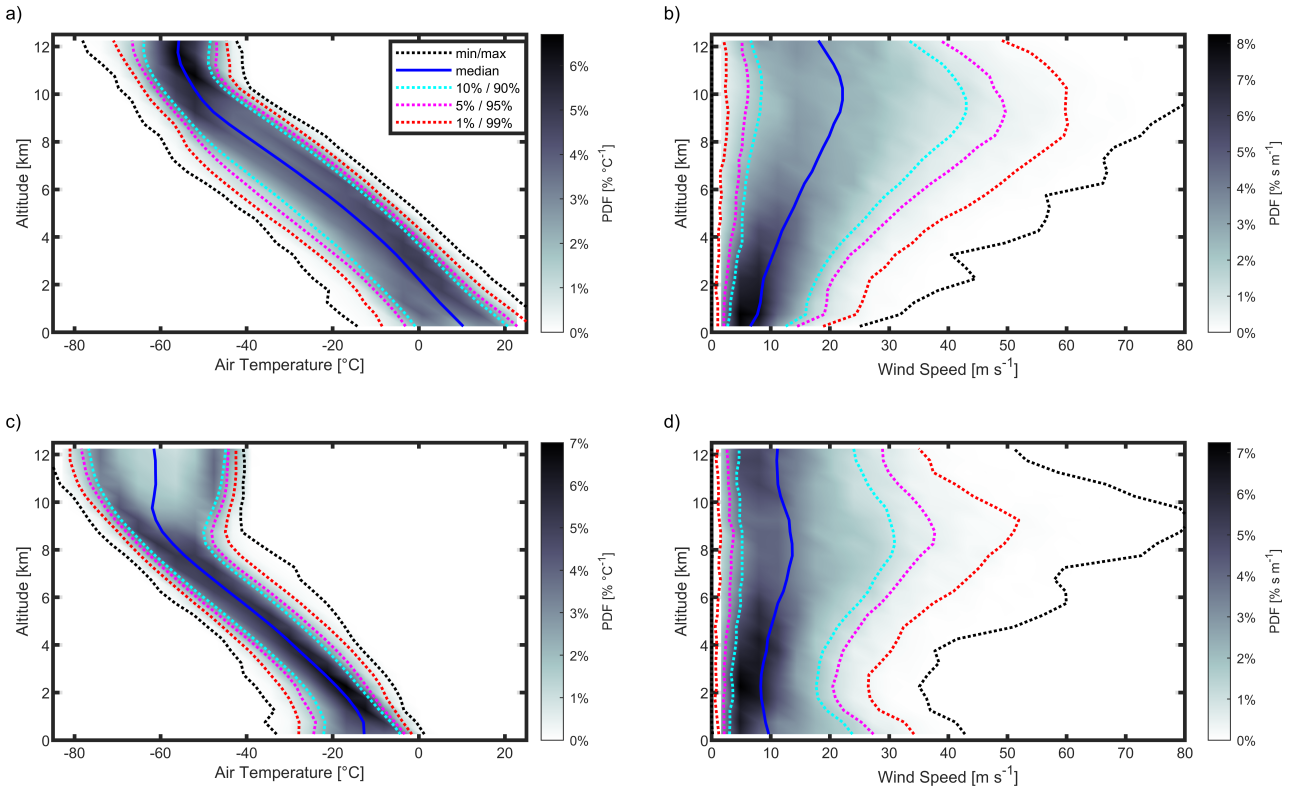

Figure 1. Analysis of environmental constraints at the radiosonde stations Lindenberg in Germany (upper panels) and Neumayer in the Antarctic (lower panels). The left panels show the probability distribution function (PDF) of air temperature with altitude in grey scale, the right panels the PDF of wind speed with altitude. The median is indicated in blue, the minimum and maximum values as black dotted line, and the percentiles including 80% (light blue), 90% (magenta) and 98% (red) of the data are indicated. The plot is based on the time period from the year 2016 to 2018, including all radiosonde launches at Neumayer around 12 UTC, and all launches around 00 UTC as well as 12 UTC at Lindenberg.

applicable to the Antarctic, but the process to determine the likelihood of icing might be used to preliminarily estimate icing frequency and icing risk for ~~UAS~~ drones in the Antarctic.

~~UAS~~ Drones are usually operated without sophisticated anti-icing and de-icing concepts like in manned aviation, in particular as most ~~UAS have been~~ drones are operated in visual line of sight. However, icing is a threat that may lead to a complete loss of the system. Icing protection for ~~UAS~~ drones has been demonstrated (Hann et al., 2021), but requires additional substantial energy for heating, even if combined with specific icephobic coatings or liquids (Huang et al., 2019).

For the demonstration flights, the ~~UAS~~ drone *LUCA* was prepared to be equipped with an icing sensor to measure in situations with a substantial risk of meeting icing conditions during the flight. Together with monitoring performance parameters, this allows estimating the severity of icing and supports the decision of abandoning the mission in icing cases. More details about the all-weather strategy is found in Bärfuss et al. (2022).

2.2 System design

Before designing the physical aircraft system, the mission to be accomplished by the ~~UAS~~ drone was defined. Although data assimilation is nowadays highly flexible regarding time, the mission was designed according to radiosonde observations to hypothetically surpass the 100 hPa surface at 12 UTC (Ingleby et al., 2022) and ensure timeliness in foresight of future inflight reporting analogue to radiosonde reporting, where a first dataset is sent to the GTS when the sonde reaches the 100 hPa level (Ingleby and Edwards, 2015). With a targeted climb rate of 10 m s^{-1} arbitrarily chosen from simple analytical estimates, the ~~UAS~~ drone has to be launched around 1133 UTC, and reaches the design ceiling of 10 km at 1150 UTC. During the flight, low frequency real time data is available. After descending with a vertical rate similar to the climb rate, an approach procedure is flown in the vicinity of the landing site to determine wind direction and wind speed, and subsequently the approach trajectory is calculated automatically on the onboard computer. After the "splashdown" into a horizontal landing net, the ~~UAS~~ drone can be recovered, and data processing including quality checks and transcoding begins. The observations of the complete flight are finally transferred into the GTS around 13 ~~:00.~~ UTC. Thus, postprocessed data from the descent profile is targeted to be available within less than an hour after the measurements are taken. Figure 2 illustrates the mission design.

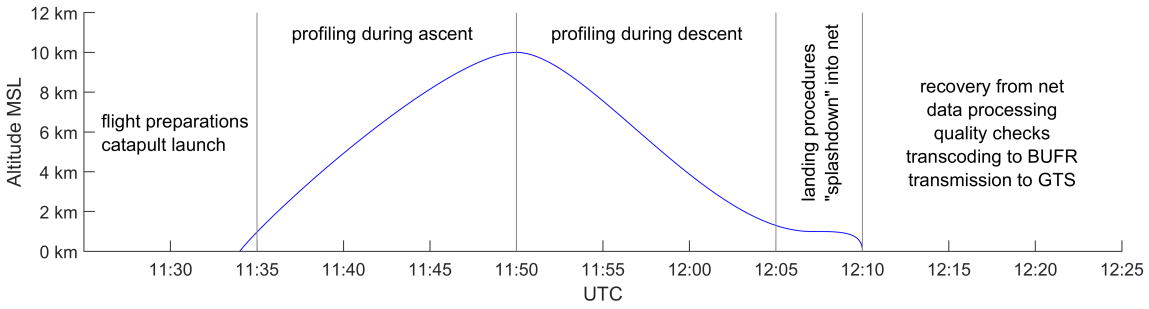

Figure 2. Mission design for the ~~UAS~~ drone *LUCA*. In order to be able to provide a first observation data set for assimilation at 12:00 UTC, the ~~UAS~~ drone is launched from the catapult at 11:33 (as shown in Figure 3a) and starts with the vertical sounding in the form of spirals at 11:35, in order to hypothetically cut the 100 hPa level at 12:00 UTC. After reaching its target altitude of 10 km at 11:50, the ~~UAS~~ drone descends with a sink rate equally to the rate of climb (10 m s^{-1}) until it arrives at the designated approach altitude around 12:05. After circles to determine the speed and direction of the near-surface wind, *LUCA* begins with the approach and lands in a horizontal landing net. Data processing, quality checks and transcoding into BUFR start directly after landing to enable data transfer of the complete flight to the GTS around 13:00 UTC.

As key design driving parameters, the ability to fly against high wind speed, an efficient electric propulsion chain and a highly flight-state independent position for the sensor package are essential. These requirements led to the development of a tailless fixed-wing configuration with a pusher propeller. As the result of a multi-variant optimization for profiling the atmosphere vertically up to 10 km, the design weighs 5-6 kg, depending on the deployed sensor package, and ~~spans~~ has a wingspan less than 2 m. Thus, the system has a minimum airspeed of 18 m s^{-1}, exceeding the minimum airspeed of crewed

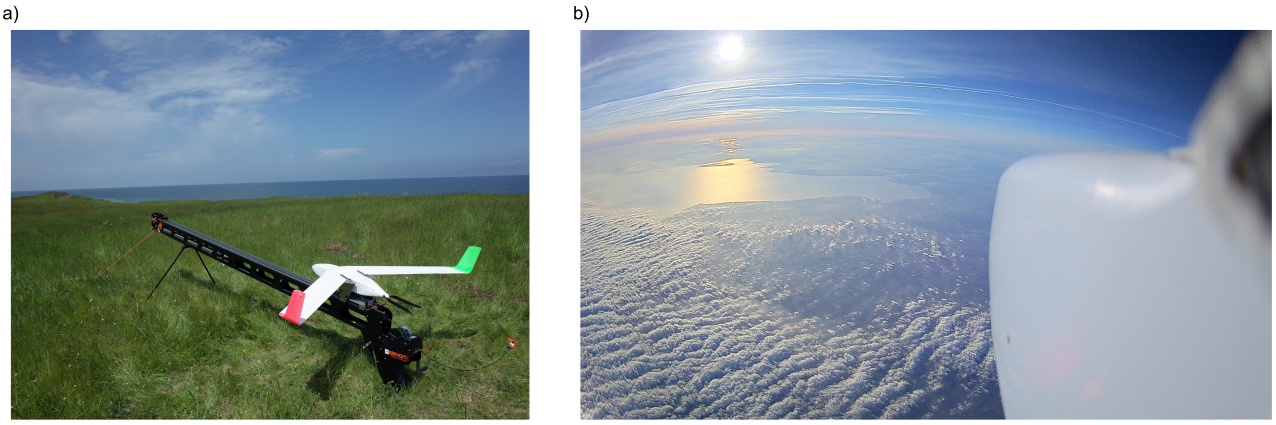

Figure 3. a) The ~~UAS~~ drone *LUCA* mounted on the catapult to get airborne for measurements over the Baltic Sea
b) A picture out of the ~~UAS~~ drone *LUCA* 10 km above the Lübecker Bight, Baltic Sea, on 28 October 2021.

ultralight aircraft. Subsequently, it is not feasible to launch the ~~UAS~~ drone by hand, and a dedicated mechanical catapult has been adapted and used during the measurement campaign (Figure 3a). ~~To support automatic landings~~As automatic take-off and landing is required for future operations in zero visibility conditions, a horizontal landing net has been developed and an appropriate maneuver to get the ~~UAS~~ drone safely into the net was implemented in the autopilot firmware (ArduPilot). The maneuver itself can be considered as ~~a vertical dive~~ an automated vertical dive into the horizontally arranged net. Whereas a belly landing is principally possible, the net landing technique was preferred as it protects the drone and the sensors from the hostile surface in the Antarctic, and prevents the system to be blown away and lost in low visibility conditions of drifting and blowing snow in case of high near-surface wind speed, as occurs frequently in the Antarctic. For the launch and retrieval system, no specific operation limits are in place regarding wind speed, as long as the launch and the landing is performed against the wind direction. Preliminary operating limits are therefore bound to the nominal airspeed of the drone. To address the risk of disintegration in turbulence, the airframe was constructed to resist gusts according to the EASA Certification Specifications 23.333 (EASA, 2022). On the avionics side, the systems on the ~~UAS~~ drone were widely predefined by national regulations (e.g. the redundancy of the command and control link).

Bärfuss et al. (2022) reveals more technical details of the drone and its ground systems, which is not the scope of this journal.

2.3 ~~Sensor~~ Simplistic sensor package

For the measurements shown, the combined resistance temperature and capacitive humidity sensor HMP110 (Vaisala, Finland) was installed within a shielded housing inside the fuselage, providing measurements of temperature and relative humidity in the closed sensing path, as sensor installation is known to influence the measurements (Jacob et al., 2018; Inoue and Sato, 2022). This sensor was previously integrated in drones, (e.g., Lampert et al., 2020; Bärfuss et al., 2021a), and its

peculiarities are well known. The enclosure furthermore protects the sensors from damage due to ground contact even during rough landings. ~~The sensor readings have been corrected by an inverse filtering method similar to the algorithm presented in Miloshevich et al. (2004). Static pressure ports and a~~An illustration of the sensor installation used for the measurement flights is provided in Figure 4a, where the measurement nose of the drone is shown. A total pressure port (Pitot tube) and static pressure ports on both sides of the drone were implemented in the nose section of *LUCA* to enable the autopilot sensors to measure ~~static and dynamic pressure. Horizontal wind components were calculated using the heading output of the~~ dynamic and static pressure. Below the pitot tube, an air inlet for the temperature/humidity probe (T/RH probe inlet) is installed. The sensor itself is mounted within the bulkhead, which separates the sensor chamber from the fuselage area. Subsequently to passing by the sensing elements, the air perfuses the measurement chamber and vents out through apertures in the bottom of the nose section (Venting). As the body of the combined temperature and humidity probe is made of stainless steel and is mounted through the bulkhead between the sensor chamber and the fuselage area, thermal conduction into the sensor chamber which might affect the measurements is expected in the case of temperature differences between the ambient air temperature and the temperature inside the fuselage, as mentioned in, e.g., Lampert et al. (2020). Additionally, the response times of the humidity measurements are expected to increase further, as the "wetted" area inside the sensor chamber is not well vented. Besides the sensors and pressure ports in the nose section, measurements of static and dynamic pressure, attitude angles, earth-related position and velocities - all taken by the autopilot system (Cube Orange, HexAero, Singapore) were recorded to derive atmospheric variables. As a drawback, the inertial navigation algorithm running on the autopilot system to calculate attitude angles, earth-related position and velocities, relies on industrial grade GNSS (Global Navigation Satellite System), rotation rate, acceleration and magnetic field sensors, which limits the accuracy of the location and attitude estimation and ~~therefore~~ subsequently limits the accuracy of the wind calculation, ~~depending on~~ varying with the flight trajectory. ~~In addition, magnetic vector measurements to be fused in the attitude estimation might be~~ Particularly heading information might be adversely deteriorated by electromagnetic interference originating from the power train~~. A camera was installed into the cutout~~ , which is more pronounced during the ascent. Additionally, the estimation filter in the inertial navigation algorithm is not able to observe sensor (e.g. turn rate sensor) errors well during flight phases with low trajectory dynamics. As an example for a flight trajectory, the measurement flight on 28 October 2021 07:20 UTC, is shown in Figure 4b. The trajectory during the measurement flight consist mainly of circular patterns, and therefore provides trajectory dynamics to facilitate the calculation of aircraft attitude, velocity and position performed by the inertial navigation algorithm.

A cut-out in the left wing ~~, which~~ is foreseen for an icing ~~detector~~sensor as shown in Bärfuss et al. (2021a), but other instruments can be fitted into it. As the risk of inflight icing was negligible during the measurements, a camera was installed into the cut out. The camera captured video and audio during the measurements, see Figure 3b, and helped to analyse the behaviour of the flight controller and the motor controller of the ~~UAS~~drone.

2.4 Permissions for operation

The most important aspects for ~~UAS~~ drone flights is safety. Operational requirements are different for each region of the world, however, in Europe, there are now unified regulations for ~~UAS~~ drone operation (EASA, 2022). The requirements concerning

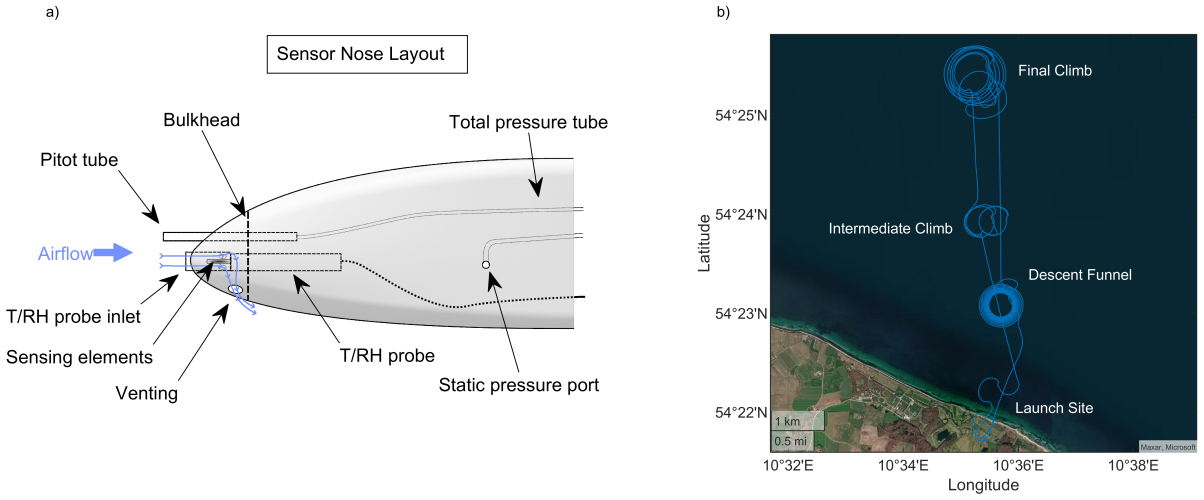

Figure 4. a) The measurement nose section with pressure ports for total pressure (Pitot tube) and static pressure (Static pressure port) and the installation of the temperature and humidity probe (T/RH probe, HMP110, Vaisala, Finland). The probe itself is mounted in the bulkhead, which separates the sensor chamber from the general fuselage area. The air enters the air inlet (T/RH probe inlet), passes the sensing element, and vents out through apertures in the bottom of the nose section (Venting).
b) Trajectory of the measurement flight on 28 October 2021 07:20 UTC - besides the launch site, the intermediate climb position where the drone climbs up to 3 km, the final climb position where it climbs up to ceiling, as well as the descent funnel are labelled.

redundancy and the level of integrity of the ~~UAS~~ drone depend on the overall risk analysis. For relatively small and light-weight ~~UAS~~ drones performing flights beyond visual line of sight, which is the case for any system operating up to an altitude of 10 km, the ~~UAS~~ drone falls in the category "specific", and precautions to avoid damage to third party have to be met. An operations handbook includes e.g. regular checks and maintenance of vital parts like motors and propellers, redundancy in the electric system, regular training of the crew, independent control links, and many more aspects defined in the so-called Operational Safety Objectives. The flight tests were therefore done in military restricted areas, in this case close to the Baltic Sea, Germany, and the internationally recognised high quality portable radiosonde system of GRAW, Germany (Nash et al., 2011) was deployed from the launching site for direct comparison. In the restricted areas, a cooperation with the German Federal Armed Forces is required, and flight permission of the German Federal Agency for Air Traffic Control (Bundesamt für Flugsicherung, BAF) is necessary.

For the operation in the Antarctic, a thorough risk assessment was performed with particular emphasis on safety and redundancy to avoid damage to third party even in such a sparsely populated area. Further, for the deployment in the Antarctic, a permission of the German Environmental Agency (Umweltbundesamt) is required, ensuring that no material stays in the pristine environment, and that the penguin population near the Neumayer Station is not disturbed.

Table 1. Sensor comparison between the radiosonde ~~, the UAS *LUCA*,~~ and the ~~prospective uncertainty of~~ drone *LUCA* using ~~an established sensor package (Bärfuss et al., 2018; Lampert et al., 2020)~~datasheet values. Calibration and removal of installation errors are an own branch of science with an increased need of effort according to data quality, e.g. for climate monitoring (Dirksen et al., 2014, 2020). Raw observation errors originating from the increasing response time of capacitive humidity sensors with decreasing temperature and the temperature corruption originating from the increased pressure at the sensing element for temperature have to be considered and possibly corrected (Bärfuss et al., 2018).

Sensor uncertainty	Radiosonde GRAW DFM-09	LUCA ~~LUCA (prospective)~~ [a)]
position	< 5 m [b)] ~~2.5 m~~ [b)] [a)]	2.5 m [b)] [a)]
pressure	< 30 Pa	< 50 Pa ~~< 30 Pa~~
temperature	< 0.2 °C	0.4 °C ~~0.1 °C~~
humidity	< 4 % RH	< 4 % RH [c)] ~~< 4 % RH~~ [c)] [b)]
wind speed	< 0.2 m s^{-1}	~~1 m s^{-1} 0.2 m s^{-1}~~ n/a [d)]
wind direction	n/a [d)] ~~10 ° [d)]~~ [c)]	~~3 °~~ n/a [d)]

[a)] slightly differing between vertical and horizontal
[b)] including non-linearity and repeatability
[c)] depending on wind speed
[d)] complex error behaviour

3 ~~Results~~

~~In the following section, the technical achievements and the resulting potential of UAS measurementsare presented. The importance of measurements up to an altitude~~

2.5 Post processing and calculi applied on data

2.5.1 Temperature corrections

The sensor readings have been corrected by an inverse filtering method similar to the algorithm presented in Miloshevich et al. (2004) which was also used prior to complementary filtering as applied in Bärfuss et al. (2018). Temperature and humidity measurements are assumed to follow the state of the atmosphere with a time lag originating by the heat/humidity capacity of the sensing element and the difference between atmospheric state and sensor state as driving for the convergence gradient, see e.g. VAISALA (2021). Such a system can be expressed by the linear differential equation

$$T \cdot \dot{y}(t) + y(t) = u(t) \tag{1}$$

where the quantity to measure is denoted with u, the measurement by y (both as a function of time t), and a time constant T. $\dot{y}$ is the derivative of $y(t)$ for t. The time constant represents the sensor response time in the way that the measurement will reach 63 % of the input state within the time span T assuming a step change on the input side. Having identified the time constant for the sensor response, signal reconstruction of the measurement time series $y(t)$ can be applied to determine the quantity

to measure $u(t)$ by applying Equation 1. As the derivative of the measurements $\dot{y}(t)$ has to be used for signal reconstruction, measurement noise will be amplified in the recovered signal, and is phase-neutrally low-pass filtered by filtering the recovered signal forward and backward. For the temperature measurements, an installation and sensor type specific time constant T_{temp} of 21 s has been identified and applied to the measurements. To correct for the heat transfer between the fuselage area and the sensor chamber, the corrected measurement T_{corr} has been assumed to behave as

$$T_{corr} = T_{recov} - (T_{fuse} - T_{recov}) \cdot m \tag{2}$$

with the recovered temperature signal T_{recov}, the temperature T_{fuse} and a dimensionless coefficient $m \approx 0.07$. An increasing difference between the measurements of the drone and the closest radiosonde can be observed above 5 km altitude without this correction. Both the time constant T_{temp} as well as the dimensionless coefficient m were estimated by comparing measurements from ascents with measurements from descents as described in Bärfuss et al. (2018).

2.5.2 Humidity corrections

The sensor principle used for humidity measurements is based on a humidity-dependant capacitive element. Such elements are well known do have an increasing response time with decreasing temperatures as e.g. shown in Choi et al. (2018); Majewski (2020) . The so called "time constant" is therefore not constant any more, and has to be applied as a variable to the signal reconstruction of the humidity measurements. For the simplistic sensor setup, an altitude dependant approximation has been adopted rather than a temperature-dependant approximation for the sake of simplicity. Reviewing literature, a power law was found to be appropriate, and using the method of comparing ascent and descent profiles, the supporting points for the function

$$T_{humi} = a \cdot H^b + c \tag{3}$$

which expresses the variable "time constant" T_{humi} for the humidity signal as a function of altitude in meters H. The parameters were estimated as T_{humi}= 15 s at 0 km, 60 s at 3 km and 2000 s at 10 km~~is shown by an analysis of the~~ . The humidity measurements are then corrected with the same recovery algorithm as applied on temperature measurements.

2.5.3 Wind calculation

The basic equation to calculate the wind vector in the geodetic coordinate system noted as $\boldsymbol{w}_g$ can be written as

$$\boldsymbol{w}_g = \boldsymbol{v}_g - \boldsymbol{u}_g \tag{4}$$

using the difference between the velocity vector of the drone $\boldsymbol{v}_g$ and the true airspeed vector $\boldsymbol{u}_g$ relative to the drone, both in the geodetic coordinate system. Additional information can be found in e.g. (WMO, 2003; Rautenberg et al., 2018; Pätzold, 2018; Bärfuss et al . As the drone *LUCA* measures the airspeed with a single pitot probe, the assumption is made, that the airspeed of the drone is aligned with the drone body - in other words, side slip angle and angle of attack are assumed to be zero. In a first step, the true airspeed has to be determined using the equation $q = 0.5 \cdot \rho |\boldsymbol{u}|^2$. As the measured pressure difference $q_{raw} = p_{total} - p_{static}$, the raw dynamic pressure suffers from pressure port errors, a calibration factor found by comparing true airspeed when flying

in different directions assuming constant mean wind is applied. For the drone *LUCA*, the calibration factor q_c/q_{raw} was found to equal 0.83 (dimensionless). Subsequently, the true airspeed $|\boldsymbol{u}|$ is corrected for the vertical velocity which involves the assumption of zero vertical wind and rotated into the geodetic coordinate system with the yaw angle of the drone, before the instantaneous wind vector is calculated using Equation 4. This equals the calculus within AMDAR (WMO, 2003), but without excluding wind measurements during aircraft bank angles above a certain threshold and with averaging over a shorter time span (less than 5 s) compared to measurements reported by AMDAR, which is 10 s. Turbulence might impact the measurements, as especially the assumptions of zero side slip angle and zero angle of attack are violated, but this effect can be eliminated by averaging over a few seconds depending on the turbulence-induced dynamics of the ~~atmosphere for the altitude range of 0–20~~drone. Besides the dynamic pressure and air density derived from the meteorological sensors, the velocity vector $\boldsymbol{v}_g$ as well as the yaw angle of the drone have to be extracted from the autopilot system. The general calculus for the wind vector, Equation 4, can be used to realise the following: For radiosondes drifting with the wind, $\boldsymbol{u}_g$ is zero, and therefore, $\boldsymbol{w}_g = \boldsymbol{v}_g$. Thinking about the ratio of true airspeed to wind speed, the retrieved wind vector gets increasingly sensitive to angular errors. This leads to the conclusion that wind observations on airliner aircraft ($|\boldsymbol{u}|^2 \approx 250\,m\,s^{-1}$) require much more accurate attitude (yaw) information to reach the same accuracy as the drone *LUCA* ($|\boldsymbol{u}|^2 \approx 28\,m\,s^{-1}$).

2.6 Methods to assess the data quality of the simplistic sensor setup

For the comparison of data obtained by *LUCA* and radiosonde data, a procedure similar to what is presented in Wagner and Petersen (2021) is applied to the data. In a first step, data within pressure bands of 5 hPa are found for drone observations and radiosonde observations. Assuming constant wind situation at the particular altitude associated with the pressure band, the air parcel measured by the radiosonde is shifted with the wind according to the time difference between the drone measurement and the radiosonde measurement. As for example the drone was measuring at 09:20 within the pressure level of 500 hPa and the radiosonde was measuring at 09:30 at the same pressure level, the radiosonde position is shifted to a virtual position by the vector, which an air parcel would have travelled within 10 minutes in the surrounding mean wind which is assumed to be constant. These virtual positions are then taken into account to select measurements collocated in space and time. The collocation conditions identical to the conditions used in Wagner and Petersen (2021) (spatial distance less than 50 km, temporal gap less than 30 min) were then applied, before measurements were intercompared. No explicit filter for outliers was applied, but the drone data was implicitly filtered for outliers by median filtering the data measured in each particular pressure band of 5 hPa width. Differences were computed for all pressure bands on all six flights.

2.7 Variability of the atmosphere

In the following, the temporal variability of temperature, wind speed and relative humidity up to 35 km is illustrated based on ERA5 reanalyses ~~data (Hersbach et al., 2018, 2020)~~to enable a discussion of the use of additional data observed with drones. To describe the variability of the atmosphere at a specific location and altitude for one parameter, time series of the atmospheric variables can be transformed from the time domain into the frequency domain e.g. by applying a Fourier transformation. Mapping the results in the frequency domain for every altitude on colors and stacking them over the corresponding altitudes

reveals the height dependent variance of an atmospheric variable on different time scales (herein, the time scale is denoted by cycles per day). E.g., a bright spot for the variable temperature at 1 cycle per day (period 24 hr) close to the surface reveals the diurnal cycle of the temperature in the boundary layer (forced by the sun). Such an analysis of temperature, humidity and wind speed is shown in Figure 5 for the location of the Lindenberg Meteorological Observatory of the German Weather Service using hourly ERA5 reanalysis data (Hersbach et al., 2018, 2020) for a timespan of one year. Similar calculations are found in Vinnichenko (1970) and Fiedler and Panofsky (1970), but in contrast to the study of Vinnichenko (1970), which focuses on the kinetic energy spectrum in the free troposphere and the study of Fiedler and Panofsky (1970), which focuses on spectral gaps, the qualitative fields presented here are used to discuss the benefit of sampling the atmosphere frequently (more than twice a day).

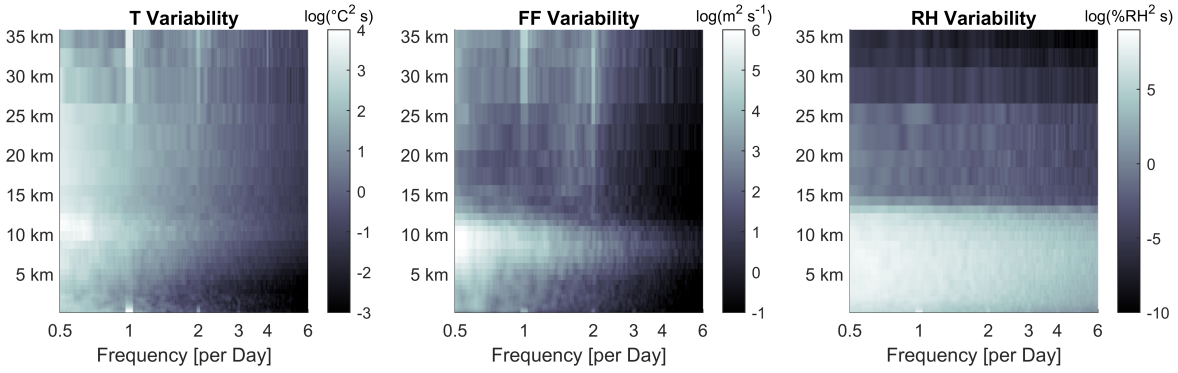

Figure 5. Color coded mesoscale (periods from 1 to 48 hr (Fiedler and Panofsky, 1970)) variance densities of time series of atmospheric variables at specific pressure levels (heights). The variances are representative for the atmospheric variability dependant on height and cycles per day (1 cycle per day corresponds to a period of 24 hr, 2 cycles per day to 12 hr). The data for this analysis origins of the ERA5 reanalysis product. Bright colors indicate high variance density and hence high variability. a) represents temperature, b) represents wind speed, and c) represents humidity. In a), one can clearly see the diurnal cycle of temperature close to the surface and in the stratosphere through the bright lines at one cycle per day. The bright lines at two cycles per day shall not confuse the reader, as the analysis relies on decomposing the time signal in sinusoids with differing frequencies (cycles per day), and higher harmonics (natural products of the fundamental frequency) reveal the non-sinusoidal waveform of the diurnal cycle. Besides in the atmospheric boundary layer, increased variability can be seen around 10 km altitude for temperature, and, after a dip in activity, around 20 km. Interestingly, temperature variability at a cycle of 6 per day is low below 5 km altitude, pronouncing the importance of profiling the atmosphere to higher altitudes.

3 Results

In the following section, the technical achievements and the resulting potential of drone measurements are presented. Therefore, data is discussed in a qualitative and a quantitative way.

3.1 Technical Achievement: First flight up to 10 km with battery powered meteorological ~~UAS~~drone

LUCA designates a new type of small fixed-wing ~~UAS~~drone. The combination of a relatively small wingspan below 2 m and a total weight of more than 6 kg leads to a high minimum flight speed of 18 m s^{-1} at sea level for obtaining the lift required to fly, and therefore complicates the process of getting airborne and landing safely compared to aircraft with larger wing area related to the total mass. During the flight test and measurement campaign, the design altitude of 10 km was reached. Ascending to such altitudes can be regarded as unique for electrically powered fixed-wing ~~UAS~~ drone without solar panels. To the authors' knowledge it is the first time that a meteorological drone powered only by electrical batteries reached the altitude of 10~~km.~~ km. In addition, the landing maneuver has been proven to be repeatable during test flights without manual control. A list of flights performed can be accessed in Bärfuss et al. (2022). During flight tests at sea level, a maximum airspeed of more than 60 m s^{-1} has been reached, indicating that the ~~UAS~~ drone is able to be operated in equally high wind speed (Pinto et al., 2021). For operations, a safety margin has been applied and the designated horizontal wind speed limit for normal operations was set to 28 m s^{-1}, which equals the ~~minimum~~ nominal horizontal component of the true airspeed during the ascent. Drifting away from the measurement location is prevented by forcing the minimum ground speed to 2 m s^{-1}. The flight controller increases automatically the airspeed ~~,~~ when the minimum ground speed falls below the threshold because of high wind speed - potentially trading the climb rate for airspeed. Resisting high wind speed and the corresponding turbulence has been demonstrated during the flight on 25 October 2021 starting at 12:12 UTC, where the maximum measured wind speed was 28 m s^{-1} (55 ~~kts~~ kn respectively) during ascent and descent at an altitude of 7800 m MSL (mean sea level). ~~To address the risk of disintegration in turbulence, the airframe was constructed to resist gusts according to the EASA Certification Specifications 23.333.~~ Operations in BVLOS (beyond visual line of sight) conditions and in the presence of closed cloud layers have been conducted successfully.~~As automatic take-off and landing is required for future operations in zero visibility conditions, procedures were developed for both cases. Take-off is realised by a catapult start. The landing maneuver consists of an automated dive into a horizontally arranged net, which has been proven to be repeatable during test flights without manual control. An article revealing technical details of the UAS, which is not the scope of this journal, will be published in an aerospace journal.~~

The drone measurements can take place from any location, up to the altitude of 10 km, if flight permission is obtained. It is completely independent of additional infrastructure, like an airport, or the availability of helium. The drone only requires a cylindrical air space with a radius of about 11 km for the whole mission. The drone ascends and descends at a vertical speed of 10 m s^{-1} and a horizontal speed component of 100 km h^{-1}. Therefore, the mission up to 10 km altitude and back to the landing site takes in total 33 min. The data is available by remote transfer with a temporal resolution of 1 Hz. The full data set with a resolution of up to 100 Hz can be downloaded after landing and is preprocessed automatically for upload into the GTS. The subsequent launch after landing can be typically performed after a turnaround time of 20 min.

3.2 ~~Comparison~~ Qualitative comparison of meteorological observations between ~~UAS~~ drone and radiosonde data

A measurement campaign with *LUCA* and radiosondes was performed at the Baltic Sea (54.4 N, 10.6 E) from 25 to 29 October 2021. An overview of the development of the meteorological conditions with altitude is shown in Figure 6 based on hourly ERA5 reanalysis data ~~(Hersbach et al., 2018, 2020)~~(Hersbach et al., 2018, 2020). The distribution of relative humidity with time and altitude was highly variable during the measurement period. Also wind speed and wind direction (indicated with wind barbs) varied with height and time. The temporal distribution of the *LUCA* flights and parallel additional radiosondes ~~can be seen~~ are indicated in the overview (Figure 6). *LUCA* was tested during a time period with high relative humidity, corresponding to cloudy conditions, and with high wind speed up to 100 knots, corresponding to 51 m s^{-1}, but the ~~UAS~~ drone was not operated at the ~~exact time of this wind speed peak~~ time of the maximum wind speed at 9 km altitude. The overall wind direction was from West with surface wind speed around 10 m s^{-1} (19 ~~kts~~kn) with absence of precipitation. Low and high scattered cloud layers were present, and a broad jet stream was forecasted just in the North of Denmark with the jet core expected at 400 km distance to the North of the measurement campaign location.

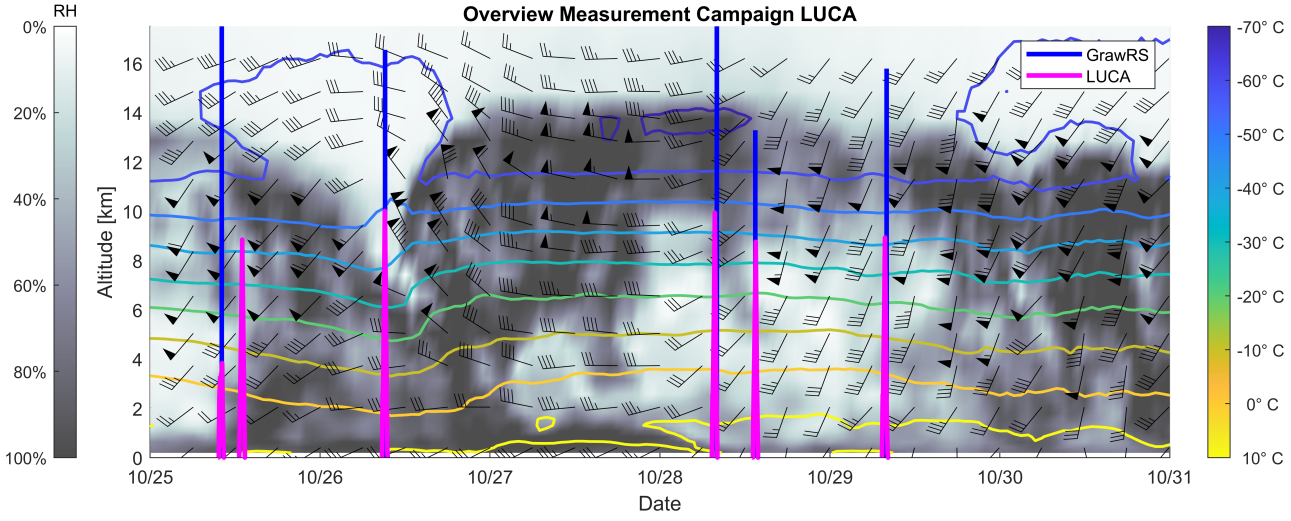

Figure 6. Overview of the meteorological situation between 25 and 31 October 2021 using ERA5 reanalysis data at the gridpoint closest to the ~~UAS~~ drone measurements. The background in grey indicates relative humidity (linearly interpolated between times and levels), whereas the colored isolines indicate air temperature. The measurement times using the ~~UAS~~ drone *LUCA* are shown in magenta, the measurements with a timely and spatially collocated radiosonde (type DFM-09, GRAW, Germany) for comparison with the ~~UAS~~ drone data is marked in blue. The wind barbs indicate the high wind speed in kn during the measurements, which coincide with the high variability in humidity over time.

~~Figure ??~~ Exemplarily, Figure 7 shows measurements of temperature, relative humidity, wind speed and wind direction recorded by *LUCA* up to 10 km. The ~~flights~~ measurements took place on ~~25~~ 26 October 2021 at ~~09:21 UTC and 10:07~~ 08:45

UTC, and on ~~26 October 2021 at 08:38 UTC. Data of the simultaneous radiosonde ascents are shown for the first and the third flight. No radiosonde was launched for direct comparison on 25~~ 29 October 2021 at ~~10:07, and therefore the dataof the radiosonde ascent launched simultaneously with the first flight on the 25 October 2021 was used for comparison. Subsequently, the profiles differ significantly due to the time gap of almost 3 hours~~07:22 UTC. The data of the nearly simultaneous radiosonde are shown as well as ERA5 reanalysis data.

Each profile provided by *LUCA* shows qualitatively the same atmospheric structures as the radiosonde measurements with a similar sensor ~~setup as in~~ package as used on the radiosondes.~~In general, the relative humidity was highly~~

On 26 October 2021, the strong temperature inversion at 400 m as well as the transition to a different temperature gradient at an altitude of around 6500 m are equally captured by the drone and the radiosonde measurements (Figure 7a). On 29 October 2021, the temperature inversion at the top of the boundary layer at 400 m altitude is captured by the drone and the radiosonde, as well as ERA5 analyses.

Humidity was generally moderately variable during the observation ~~periods. All measurements~~period. The drone and radiosonde measurements, as well as ERA5 data agree that there was high relative humidity (small differences between dew point temperature and temperature) up to the temperature inversion at around ~~1~~400 ~~km for~~ m altitude on 26 October 2021 (Figure 7a). On both days, ~~followed by several layers of enhanced relative humidity, a relatively dry altitude range between~~ there were layer of lower and higher humidity. On 26 October 2021, in the lower troposphere up to an altitude of ~~3 km and 5-6~~around 4 km, ~~and again a layer of enhanced relative humidity above. In the lower troposphere, fine layers of~~ the individual layers of different humidity are identically resolved by the ~~UAS~~ drone in altitude and magnitude ~~as it is shown in Figure ??a, and the temperature inversion at the top of the boundary layer at 800 m has been captured by the system. These features are also obvious in the measurements of the simultaneously launched radiosonde. Figure ??b shows measurements 3 hours later than the measurements in Figure ??aand indicates fast changes of the atmospheric parameters during the measurement period. In Figure ??c, relative~~ (Figure 7a). On 29 October 2021, humidity measurements using the ~~UAS~~ drone are in good agreement with radiosonde data up to 500 hPa (around 5 km altitude, Figure 7b). Above 500 hPa, an increasing deviation between radiosonde and ~~UAS~~ drone measurements can be observed in ~~relative humidity~~ humidity for both days. This is likely caused by the dramatically increasing response time of the humidity sensor at lower temperatures ~~(Choi et al., 2018)~~ (Choi et al., 2018; Majewski, 2020) in addition to the delaying effect of the implemented closed path sensor setup. Moisture is ~~known as~~ a critical parameter to measure in the upper troposphere (Nash et al., 2011; Dupont et al., 2020).~~The temperature inversion at 400 m as well as the transition to a different temperature gradient at an altitude of around 6500 m on 26 October 2021 are equally captured by the UAS and the radiosonde measurements. An increasing difference between the measurements of the UAS and the radiosonde can be observed above 5 km altitude. This is likely caused by heat transfer inside the fuselage to the sensor head. Wind measurements are consistent between the UAS~~

Wind measurements agree well between the drone and the radiosonde measurements~~and demonstrate directly the ability of *LUCA* to operate in high wind speed. Furthermore, UAS wind measurements provide additional information about turbulence, since the wind vector is derived multiple times per second~~. When comparing the measurements directly, one has to take in ac-

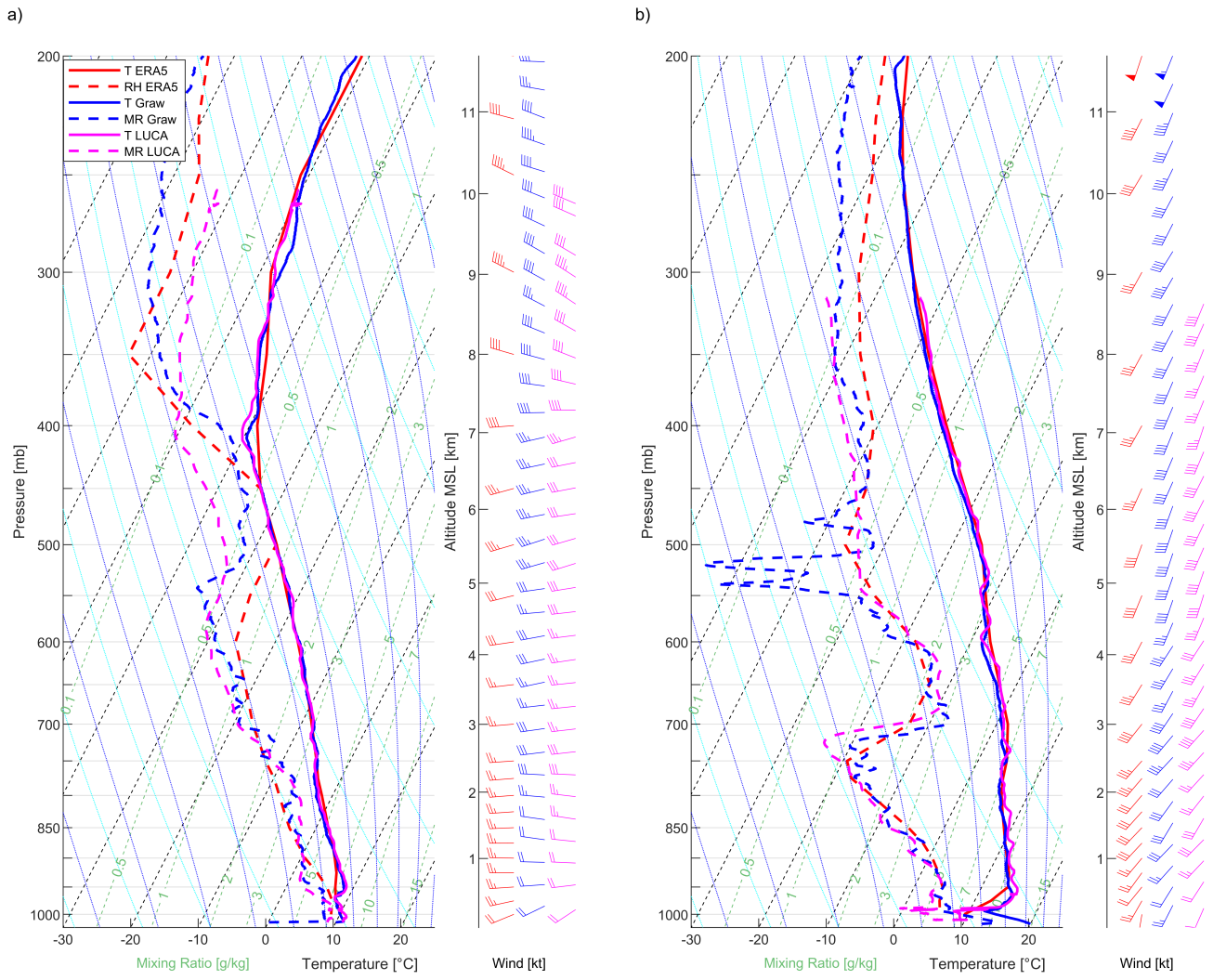

Figure 7. Skew-T Log-p diagrams of the vertical profiles (descent) of temperature (solid lines), dew point temperature (dashed lines) and wind (wind barbs, in kn) measured with *LUCA* in magenta~~and for cases a) and c)~~ , with the simultaneously launched radiosonde in blue, and ERA5-Data in red. In a), the launch time of *LUCA* was ~~09~~08:~~21~~ 45 UTC on ~~25~~ 26 October 2021, and the radiosonde ~~on the same day~~ was released at ~~10~~09:~~07~~ 11 UTC. ~~In b), the UAS~~ The drone profile was ~~launched at 12~~measured during the descent from 09:~~12~~ 09 to 09:30 UTC~~on 25 October 2021 and the same radiosonde as for a) was used~~. In ~~c~~b), ~~*LUCA*~~ the drone was launched at ~~08~~07:~~38~~ 22 UTC on ~~26~~ 29 October 2021 ~~,~~and the corresponding radiosonde was released at ~~09~~08:~~11~~ 01 UTC. The drone profile was measured during the descent from 07:47 to 08:12 UTC.

count that the radiosonde was launched 53 min after the ~~UAS~~drone. A systematic deviation can be expected for higher altitudes

due to the drifting of the radiosonde with the wind, therefore towards North-East, which resulted in a spatial distance of 40 km from the launch point when reaching the altitude of 10 km.

3.3 ~~Potential for covering data gaps with UAS based on atmospheric dynamicsThe UAS has the capability of measuring frequently, e.g. hourly. More frequent observations increase the forecast quality (Faccani et al., 2009; Dabberdt et al., 2005), as special atmospheric features like the diurnal cycle can be resolved. The required frequency of measurements strongly depends on the temporal variability of the atmosphere, which is highly variable for different altitude ranges, and different for each meteorological parameter. In the following,~~ Case study: Quantitative intercomparison of the ~~temporal variability of temperature, wind speed~~ simplistic sensor setup and ~~relative humidity up to 35~~radiosonde data

Despite the simplistic sensor setup, data measured onboard the platform *LUCA* has shown to compare at least qualitatively with radiosonde data. To assess qantitative measures, the methods presented in Section 2.6 are applied on the data postprocessed according to Section 2.5. These techniques were applied for ascents as well as descents, as data during the ascent is expected to suffer from electromagnetic interference as well as other treats such as thrust line misalignment. The collocated dataset for the pressure bands of 2 ~~km is investigated based on ERA5 reanalyses. To describe the dynamics of the atmosphere at a specific location and altitude for one parameter, time series of the parameter can be transformed from the time domain into the frequency domain (Fiedler and Panofsky, 1970; Vinnichenko, 1970) e.g. by applying a Fourier transformation. Mapping the results in the frequency domain for every altitude on colors and stacking them over the corresponding altitudes reveals the height dependent variance of an atmospheric parameter on different time scales (herein, the time scale is denoted by cycles per day). E. g. a bright spot for the variable temperature at 1 cycle per day (period 24 hr)close to the surface reveals the diurnal cycle of the temperature in the boundary layer (forced by the sun) . Such an analysis of temperature, humidity and wind speed is shown in Figure 5 for the location of the Lindenberg Meteorological Observatory of the German Weather Service using hourly ERA5 reanalysis data (Hersbach et al., 2018, 2020) for a timespan of one year.~~hPa width from 1000 hPa to 250 hPa consists of 694 data points for the ascent and 1323 data points for the descent of the drone. Figure 8 shows histograms of the differences between the radiosonde observations and the drone observations for the variables temperature, relative humidity, specific humidity, wind speed, wind direction as well as the norm of the wind vector difference for the descending profiles. Within the histograms, average differences as well as the standard deviation of the intercompared observations is provided.

~~As one would expect,~~ Despite the sparse database consisting of six vertical descent profiles, the differences for the variables temperature, relative humidity, specific humidity, wind speed and wind direction are similar to Gaussian distributions. The histogram for the norm of the wind vector difference follows a Rayleigh distribution, as it is expected for the norm of a two dimensional vector, whose components are stochastically independent Gaussian processes. For the distribution of the observation differences, the average deviation as well as the standard deviation (root-mean-squared-error for the Rayleigh distribution) were calculated and shown in the histogram plots (Figure 8). These values were retrieved for both the ascent and the descent, and are shown in Table 2.

~~Color coded mesoscale (periods from 1 to 48 hr (Fiedler and Panofsky, 1970)) variance densities of time series of atmospheric variables at specific pressure levels (heights). The variances are representative for the atmospheric variability dependant on height and cycles per day (1 cycle per day corresponds to a period of 24 hr, 2 cycles per day to 12 hr). The data for this analysis origins of the ERA5 reanalysis product. Bright colors indicate high variance density and hence high variability. a) represents temperature, b) represents wind speed, and c) represents humidity. In a), one can clearly see the diurnal cycle of temperature close to the surface and in the stratosphere through the bright lines at one cycle per day. The bright lines at two cycles per day shall not confuse the reader, as the analysis relies on decomposing the time signal in sinusoids with differing frequencies (cycles per day), and higher harmonics (natural products of the fundamental frequency) reveal the non-sinusoidal waveform of the diurnal cycle. Besides in the atmospheric boundary layer, increased variability can be seen around 10 km altitude for temperature, and, after a dip in activity, around 20 km. Interestingly, temperature variability at a cycle of 6 per day is low below 5 km altitude, pronouncing the importance of profiling the atmosphere to higher altitudes.~~

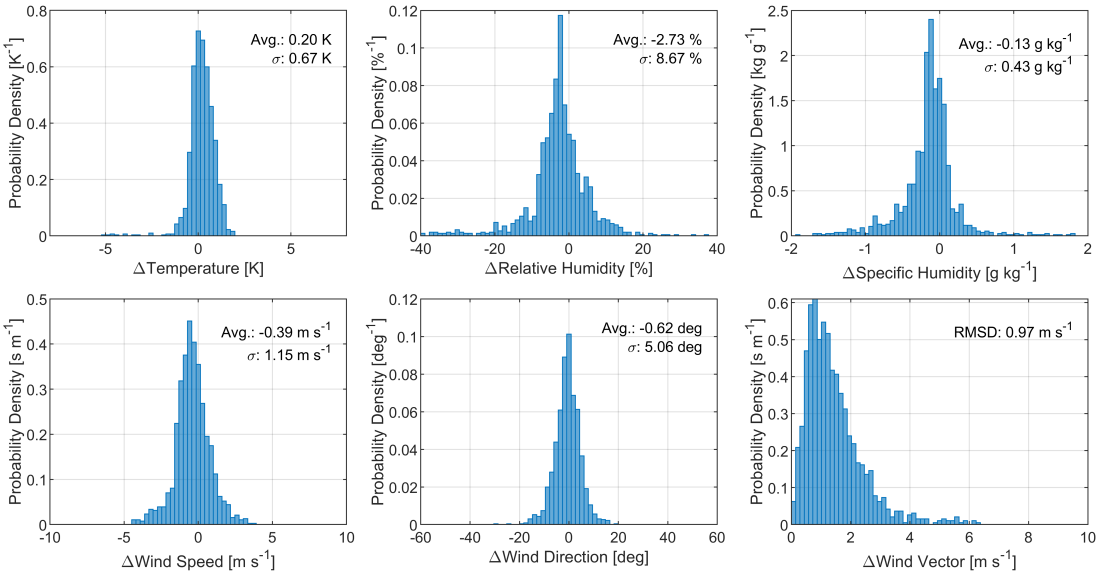

Figure 8. Histograms (probability density over observation difference) of the differences between collocated drone *LUCA* and radiosonde observations for various atmospheric variables. Collocation was assumed for the probed air parcels virtual spacial distance of less than 50 km and an observation time difference of less than 30 min. The virtual air parcel position was determined by virtually back-shifting the probed air parcel with the negative mean wind vector at the observation level multiplied with the time difference between the drone and the radiosonde measurements within the same pressure level band. All histograms suffer from the sparse database, but indicate a Gaussian-like distribution of observation differences, except the difference of the wind vectors, which follows a Rayleigh distribution as expected from theory. Therefore, the RMSD is shown on the histogram for the wind vector difference rather than standard deviation as for the other parameters.

Comparing the statistical measures between ascent and descent data, increased differences between the radiosonde observations and the drone observations are revealed. This is most likely associated with a magnetic deterioration or a possibly induced side slip angle when the thrust line is not aligned with the drone's body (see Sections 2.3 and 2.5.3). For the descent profile, the

Table 2. Statistical measures for the differences in the collocated observation of temperature, humidity and wind between drone measurements and radiosonde measurements. Collocation was assumed when an air parcel, virtually reverse-shifted by the mean wind and the time difference, was within a spatial distance of less than 50 km and a temporal difference of less than 30 min. The statistical measures are shown for both the descent as well the ascent profile compared to radiosonde data. During the ascent profile, an increased variation in wind observation, particularly wind direction, can be found compared to the descent profile. Despite the simplistic sensor setup on the drone, average difference as well as the standard deviation is less than average differences and standard deviations from an intercomparison of airliner observations and radiosondes. This indicates a possibly higher accuracy of the drone observations than observations within the AMDAR/TAMDAR programme.

	Descent		Ascent	
Variable	Average	$\sigma^{a)}$	Average	$\sigma^{a)}$
Temperature	0.20 K	0.67 K	0.00 K	0.86 K
Relative Humidity	2.73 %	8.67 %	-4.64 %	8.16 %
Specific Humidity	-0.13 g kg^{-1}	0.43 g kg^{-1}	-0.30 g kg^{-1}	0.53 g kg^{-1}
Wind Speed	-0.39 m s^{-1}	1.15 m s^{-1}	-0.40 m s^{-1}	2.66 m s^{-1}
Wind Direction	-0.62 deg	5.06 deg	-0.77 deg	21.88 deg
Wind Vector	n/a	0.97 m s^{-1}	n/a	2.66 m s^{-1}
Database Info	1323 data points (68 % of dataset)		694 data points (35 % of dataset)	

$^{a)}$ RMSD for the Wind Vector difference

average differences as well as the standard deviation of the differences between drone observations and radiosonde observations are in the range (or even below) statistical measures shown in the study of Wagner and Petersen (2021), which includes a comparison of radiosonde data with observation data from the AMDAR/TAMDAR programme. This indicates a possibly higher accuracy of the drone observations compared to operational airliner observations already assimilated into NWP models, despite the simplistic sensor setup used.

4 Discussion and Conclusion

The in-situ data gap in the Global Observing System has been reviewed in the introduction. Experiments on the impact of additional vertical profiles on NWP suggest that in-situ observations of the complete tropospheric column in remote areas improve forecast quality, as well as more frequent sampling of the atmosphere would do. Besides the effort in filling the observation gap in the near-surface boundary layer with drones (Leuenberger et al., 2020; Pinto et al., 2021; Inoue and Sato, 2022), the data gap with drone measurements in the free troposphere and the lower stratosphere has not been addressed - the technology of small drones has not yet been ready for observations at such high altitudes (Geerts et al., 2018; Pinto et al., 2021).

The drone measurements presented here show the potential for covering data gaps as the drone has the capability of measuring

frequently, e.g. hourly, with moderate cost and effort. More frequent observations increase the forecast quality (Dabberdt et al., 2005; Facca
, as special atmospheric features like the diurnal cycle can be resolved. The required frequency of measurements strongly depends on the temporal variability of the atmosphere, which is highly variable for different altitude ranges, and different for each meteorological parameter, as shown in Figure 5. The atmospheric boundary layer experiences high temporal changes in temperature, wind speed and humidity. Besides ~~the~~ these diurnal variations in the lowermost region, temporal changes in temperature and wind speed are seen in the upper troposphere and the lower stratosphere. Processes in this layer ± 5 km around the tropopause (the virtual boundary between the troposphere and the stratosphere, e.g. Gettelman et al., 2011) are known as being important for global (mass) exchange (Holton et al., 1995). Humidity~~in contradiction~~ , in contrast, varies highly from the ground up to the lower stratosphere with no preference on timescales, representing a chaotic system.

Interestingly, temperature variability at a cycle of 6 per day is low below 5 km altitude (besides the high variability in the boundary layer), pronouncing the importance of profiling the atmosphere to higher altitudes. In NWP, physical processes are modeled to predict a future atmospheric state. The modelling of these processes perform quite well on distinct timescales to reproduce the variability of the atmosphere. The need for observations can therefore not only be defined by the atmospheric variability to avoid undersampling, but rather has to be seen complementary to the stability of the modeled physical processes and regional data gaps. Specified by data users, the WMO provides data requirements for observation spacing and uncertainty (WMO, 2015b; Leuenberger et al., 2020), which interestingly differ only little between the boundary layer and the free troposphere for both global and high resolution NWP, emphasizing the benefits of profiling the atmosphere vertically with a ~~UAS~~ drone up to approximately 10 km and above. Filling the in-situ observation gap both in the atmospheric boundary layer and the free troposphere ~~likely results in much~~ will result in better forecast quality and even has the potential to further adjust and develop the modelling of the underlying physical processes.

~~The in-situ data gap in the Global Observing System has been reviewed in the introduction. Experiments on the impact of vertical profiles on NWP suggest that in-situ observations of the complete tropospheric column in remote areas improve forecast quality, as well as more frequent sampling of the atmosphere would do so. Besides the effort in filling the observation gap in the near-surface boundary layer with UAS (Pinto et al., 2021; Leuenberger et al., 2020; Inoue and Sato, 2022), the data gap with UAS measurements in the free troposphere and the lower stratosphere has not been addressed - the technology of small UAS has not yet been ready for observing at such high altitudes (Geerts et al., 2018; Pinto et al., 2021).~~

This article presents atmospheric soundings up to 10 km altitude using an electrically powered fixed-wing drone. The developed system ~~demonstrates~~ represents a milestone, demonstrating the capability of fixed-wing ~~UAS~~ drones to perform tropospheric soundings~~, and measurements~~ . Measurements with a basic atmospheric sensor package were conducted. The ~~UAS~~ drone measurements of temperature, humidity and wind reported here generally agree with temporally and spatially coinciding radiosonde measurements. Minor drawbacks in the measurements occurred as expected due to the simple sensor setup.

Moisture is generally the most challenging parameter of in-flight atmospheric observations, which demands significant post-processing. This is also a known issue for standard radiosonde systems where various corrections need to be applied as well (Dirksen et al., 2014). ~~Using a more sophisticated measurement package, standard radiosonde accuracy is expected to be reached or even surpassed.~~ By design, the ~~UAS~~ drone technology bears the pivotal advantage of re-using sensors and the pos-

sibility of pre- and post-flight calibration.

More advanced sensor techniques that are available could easily be integrated into this platform. This enables to extend the measured parameters or focus on high quality measurements of basic atmospheric parameters, e.g. by using dew point mirrors for humidity (Fujiwara et al., 2003) or fine wire temperature sensors with ~~sophisticated~~ suitable shielding and protection (Stickney et al., 1994; Bärfuss et al., 2018). As an outlook, standard radiosonde accuracy is expected to be reached or even surpassed using a more sophisticated measurement package instead of the simplistic sensor integration used within this study. Sensor limitations and challenges are known, the needs regarding data management (Wyngaard et al., 2019) are not addressed within this article.

The system *LUCA* was designed to reach its target altitude (10 km) in conditions with continuous wind speed of up to 28 m s^{-1} (54 ~~kts~~kn) which results in a minimum flight speed of 18 m s^{-1}. In order to ensure the aforementioned operability, *LUCA* was constructed with suitable ground systems for take-off and landing. The mechanical start catapult enables robust starts, even in challenging conditions of high wind speed and virtually zero horizontal visibility. The landing net was designed for an automated landing manoeuvre, which allows for landings during high surface wind and low visibility conditions.

As for now, *LUCA* does not incorporate measures to actually prevent icing, but features a dedicated sensor to detect icing. This enables save operations of the flights, but limits the operability significantly. In future developments this issue needs further attention.

The reported flights that were carried out demonstrate the general suitability of the technology for the envisaged purpose, explicitly covering rather challenging environmental conditions. However, systematic and extensive tests in adverse weather still need to be performed in the future. Nevertheless, the system *LUCA* was successfully operated above the design wind speed and through closed cloud layers.

Data quality assessed within a case study using a simple sensor package indicates observation accuracy comparable to AMDAR and TAMDAR observations, but further studies have to be carried out, as the observations within the case study covers only limited atmospheric conditions.

Receiving permissions for ~~UAS~~ drone operations beyond visual line of sight is a demanding prerequisite for atmospheric measurement systems like *LUCA*. With its design mass of 5-6 kg *LUCA* is fairly light compared to crewed aircraft, but significantly heavier than typical radiosondes. Hence, the operational risk is an issue. By further miniaturisation of the system, both air and ground risk can be reduced, and hence is expected to simplify the process of granting permissions.

Compared to existing in-situ observing systems, the vertical profiles are similar to radiosonde ascents and descents (in some NWP centers, radiosonde descents are already assimilated, Ingleby et al., 2022) and aircraft based observations close to airports. Assimilation of ~~UAS~~ drone data in the BUFR format (Ingleby and Edwards, 2015; Ingleby et al., 2022) shall therefore be quite straightforward compared to new and complex assimilation processes of e.g. radio occultation data (Eyre, 2008). In comparison with observations from crewed aircraft, ~~UAS~~ drones typically operate at a lower airspeed, which tends to result in an increased wind observation accuracy (Pätzold, 2018). Even though reaching 10 km can never replace the well established radiosonde network, the system bears the chance to augment radiosoundings with more frequent ~~UAS~~ drone measurements. Furthermore, in the future it might be feasible to setup atmospheric in-situ monitoring programs by combining profiling ~~UAS~~

drones as the one presented here with solar powered semi-permanent systems in the stratosphere.

There are several possible applications and opportunities for the use of small ~~UAS~~ drones measuring the complete tropospheric column and potentially the lower stratosphere - sampling the atmosphere with an increased number of observations per day with re-usable individual sensors has to be highlighted here. Re-using sensors inevitably leads to substantial knowledge about stability, strengths and flaws of an individual sensor, and bears the chance of increasing the ability to precisely specify the uncertainty of observations, which is substantial for data assimilation. This effect is regularly observed regarding satellite sensors assessments (Rennie et al., 2021).

The use of reference radiosondes to characterize the uncertainty of NWP models to improve satellite validation and calibration is ~~an application (Carminati et al., 2019) , to which UAS~~ another future application (Carminati et al., 2019) to which drone measurements potentially can contribute. The quality of ~~UAS~~ drone observations for sampling the complete troposphere is of superior importance, and could possibly contribute to climate applications. Regarding the involved variables, one finds that climate users tend to focus on temperature and humidity data (Ingleby et al., 2022).

For NWP applications, wind has arguably more than twice the impact on the quality of short range forecast (Ingleby et al., 2021). In order to augment and compete with the well established vertical profile observations (radiosondes, ~~ABO~~airliner-borne) and being used operationally, a ~~UAS~~ drone must be operable by station staff of existing atmospheric observatories. Furthermore, the system needs to cope with a variety of challenging environmental conditions, including high wind speed, poor surface visibility or icing during the flight.

Upcoming implementations of such systems in the GTS will likely depend on investment cost as well as cost generated by the effort for station staff in respect to operations and maintenance. An generic approach to assess the economical benefit for drone based observations is presented in Bärfuss et al. (2022), but acquisition cost is unclear for the system presented here.

Targeted observations were discussed controversially, as their impact strongly depends on the assimilation scheme and the NWP system (Schindler et al., 2020). Unquestionable is the use of ~~UAS~~ drone measurements in contributing to scientific campaigns and the resulting reduction of cost and waste when used to replace frequent radiosoundings during intense observation periods.

~~Envisaged~~ Although this study demonstrates the feasibility of using small drones up to the troposphere as carrier systems for atmospheric observations, envisaged extensive test campaigns (like the WMO UAS Demonstration Campaign, WMO, 2022) are needed to assess the impact of ~~UAS~~ drones in forecast skills and shall increase and demonstrate the reliability of *LUCA* performing ~~reliable~~ successful and safe tropospheric profiling.

Data availability. The data will be published at PANGAEA. Similar data sets obtained with *LUCA* up to an altitude of 4.5 km are already publicly available (Bärfuss et al., 2021a) together with radiosonde data obtained during parallel launches (Bärfuss et al., 2021b).

Author contributions. A.L. and H.S. developed the project idea and acquired funding. H.S. performed the analysis of requirements. K.B. developed the system *LUCA* and the instrumentation. K.B. performed the data processing and data analysis. All authors contributed to and reviewed the manuscript.

Competing interests. The authors declare no competing interests.

Acknowledgements. The project AEROMET_UAV was funded by the Modernity Fund (mFUND) of the Federal Ministry for Digital and Transport (BMDV) under grant 19F2072A. The results as presented within Figures 5, 6 and 7 contain modified Copernicus Climate Change Service information ~~2022.~~ 2022 (ERA5 reanalysis data for temperature, wind and moisture). Neither the European Commission nor ECMWF is responsible for any use that may be made of the Copernicus information or data it contains. The authors would like to thank Harald Schüßler (more than scale composite); Ruud Dirksen (DWD); David Burzynski, Stephan Bansmer and Juan Velandia (Coldsense Technologies); Rolf Zimmermann and Markus Landeck (Ing.-Büros); Hans-Jürgen Unverferth (Zanonia-Flyers); Valentin Möller and Alex Helbing (Exabotix); Samira Terzenbach (AWI); and the colleagues and students at TU Braunschweig who supported the project, Heiko Wickboldt, Lutz Bretschneider, Magnus Asmussen, Andreas Schlerf, Falk Pätzold, Thomas Rausch, Sven Bollmann, Tom Schwarting and Maximilian von Unwerth. The authors would also like to thank the team of the military training ground Putlos/Todendorf under the direction of Hptm Johanssen, in particular Hptm Lucht, Kurylak and Link, for their kind assistance during the test flights.

References

Archer, C. L. and Caldeira, K.: Historical Trends in the Jet Streams, Geophysical Research Letters, 35, https://doi.org/10.1029/2008GL033614, 2008.

Baker, W. E., Atlas, R., Cardinali, C., Clement, A., Emmitt, G. D., Gentry, B. M., Hardesty, R. M., Källén, E., Kavaya, M. J., Langland, R., Ma, Z., Masutani, M., McCarty, W., Pierce, R. B., Pu, Z., Riishojgaard, L. P., Ryan, J., Tucker, S., Weissmann, M., and Yoe, J. G.: Lidar-Measured Wind Profiles: The Missing Link in the Global Observing System, Bulletin of the American Meteorological Society, 95, 543–564, https://doi.org/10.1175/BAMS-D-12-00164.1, 2014.

Bärfuss, K., Pätzold, F., Altstädter, B., Kathe, E., Nowak, S., Bretschneider, L., Bestmann, U., and Lampert, A.: New Setup of the UAS ALADINA for Measuring Boundary Layer Properties, Atmospheric Particles and Solar Radiation, Atmosphere, 9, 28, https://doi.org/10.3390/atmos9010028, 2018.

Bärfuss, K., Schmithüsen, H., Dirksen, R., Bretschneider, L., Pätzold, F., Bollmann, S., Wickboldt, H., von Unwerth, M., Asmussen, M., Schwarting, T., and Lampert, A.: Atmospheric Profile Measurements Conducted by the Unmanned Aerial System LUCA (Panker, Germany 2020-07-03 and 2021-05-28), https://doi.org/10.1594/PANGAEA.937555, 2021a.

Bärfuss, K., Schmithüsen, H., Dirksen, R., Bretschneider, L., Pätzold, F., Bollmann, S., Wickboldt, H., von Unwerth, M., Asmussen, M., Schwarting, T., and Lampert, A.: Radiosonde Measurements Co-Located with Ascends of the Unmanned Aerial System LUCA (Panker, Germany 2020-07-03 and 2021-05-28), https://doi.org/10.1594/PANGAEA.937556, 2021b.

Bärfuss, K. B., Schmithüsen, H., and Lampert, A.: Drone-Based Meteorological Observations up to the Tropopause, Atmospheric Measurement Techniques Discussions, pp. 1–26, https://doi.org/10.5194/amt-2022-236, 2022.

Bauer, P., Thorpe, A., and Brunet, G.: The Quiet Revolution of Numerical Weather Prediction, Nature, 525, 47–55, https://doi.org/10.1038/nature14956, 2015.

Bonavita, M., Hólm, E., Isaksen, L., and Fisher, M.: The Evolution of the ECMWF Hybrid Data Assimilation System, Quarterly Journal of the Royal Meteorological Society, 142, 287–303, https://doi.org/10.1002/qj.2652, 2016.

Bormann, N., Lawrence, H., Farnan, J., and Farnan, J.: Global Observing System Experiments in the ECMWF Assimilation System, https://doi.org/10.21957/sr184iyz, 2019.

Bouttier, F. and Kelly, G.: Observing-System Experiments in the ECMWF 4D-Var Data Assimilation System, Quarterly Journal of the Royal Meteorological Society, 127, 1469–1488, https://doi.org/10.1002/qj.49712757419, 2001.

Boylan, P., Wang, J., Cohn, S. A., Fetzer, E., Maddy, E. S., and Wong, S.: Validation of AIRS Version 6 Temperature Profiles and Surface-Based Inversions over Antarctica Using Concordiasi Dropsonde Data, Journal of Geophysical Research: Atmospheres, 120, 992–1007, https://doi.org/10.1002/2014JD022551, 2015.

Cardinali, C.: Monitoring the Observation Impact on the Short-Range Forecast, Quarterly Journal of the Royal Meteorological Society, 135, 239–250, https://doi.org/10.1002/qj.366, 2009.

Cardinali, C.: Observation Impact on the Short Range Forecast, https://www.ecmwf.int/node/16937, 2013.

Carminati, F., Migliorini, S., Ingleby, B., Bell, W., Lawrence, H., Newman, S., Hocking, J., and Smith, A.: Using Reference Radiosondes to Characterise NWP Model Uncertainty for Improved Satellite Calibration and Validation, Atmospheric Measurement Techniques, 12, 83–106, https://doi.org/10.5194/amt-12-83-2019, 2019.

Chander, G., Hewison, T. J., Fox, N., Wu, X., Xiong, X., and Blackwell, W. J.: Overview of Intercalibration of Satellite Instruments, IEEE Transactions on Geoscience and Remote Sensing, 51, 1056–1080, https://doi.org/10.1109/TGRS.2012.2228654, 2013.

Chilson, P. B., Bell, T. M., Brewster, K. A., Britto Hupsel de Azevedo, G., Carr, F. H., Carson, K., Doyle, W., Fiebrich, C. A., Greene, B. R., Grimsley, J. L., Kanneganti, S. T., Martin, J., Moore, A., Palmer, R. D., Pillar-Little, E. A., Salazar-Cerreno, J. L., Segales, A. R., Weber, M. E., Yeary, M., and Droegemeier, K. K.: Moving towards a Network of Autonomous UAS Atmospheric Profiling Stations for Observations in the Earth's Lower Atmosphere: The 3D Mesonet Concept, Sensors, 19, 2720, https://doi.org/10.3390/s19122720, 2019.

Choi, B. I., Lee, S.-W., Woo, S.-B., Kim, J. C., Kim, Y.-G., and Yang, S. G.: Evaluation of Radiosonde Humidity Sensors at Low Temperature Using Ultralow-Temperature Humidity Chamber, in: Advances in Science and Research, vol. 15, pp. 207–212, Copernicus GmbH, https://doi.org/10.5194/asr-15-207-2018, 2018.

Cione, J. J., Bryan, G. H., Dobosy, R., Zhang, J. A., de Boer, G., Aksoy, A., Wadler, J. B., Kalina, E. A., Dahl, B. A., Ryan, K., Neuhaus, J., Dumas, E., Marks, F. D., Farber, A. M., Hock, T., and Chen, X.: Eye of the Storm: Observing Hurricanes with a Small Unmanned Aircraft System, Bulletin of the American Meteorological Society, 101, E186–E205, https://doi.org/10.1175/BAMS-D-19-0169.1, 2020.

Cohn, S. A., Hock, T., Cocquerez, P., Wang, J., Rabier, F., Parsons, D., Harr, P., Wu, C.-C., Drobinski, P., Karbou, F., Vénel, S., Vargas, A., Fourrié, N., Saint-Ramond, N., Guidard, V., Doerenbecher, A., Hsu, H.-H., Lin, P.-H., Chou, M.-D., Redelsperger, J.-L., Martin, C., Fox, J., Potts, N., Young, K., and Cole, H.: Driftsondes: Providing In Situ Long-Duration Dropsonde Observations over Remote Regions, Bulletin of the American Meteorological Society, 94, 1661–1674, https://doi.org/10.1175/BAMS-D-12-00075.1, 2013.

Dabberdt, W. F., Schlatter, T. W., Carr, F. H., Friday, E. W. J., Jorgensen, D., Koch, S., Pirone, M., Ralph, F. M., Sun, J., Welsh, P., Wilson, J. W., and Zou, X.: Multifunctional Mesoscale Observing Networks, Bulletin of the American Meteorological Society, 86, 961–982, https://doi.org/10.1175/BAMS-86-7-961, 2005.

de Boer, G., Diehl, C., Jacob, J., Houston, A., Smith, S. W., Chilson, P., Schmale, D. G., Intrieri, J., Pinto, J., Elston, J., Brus, D., Kemppinen, O., Clark, A., Lawrence, D., Bailey, S. C. C., Sama, M. P., Frazier, A., Crick, C., Natalie, V., Pillar-Little, E., Klein, P., Waugh, S., Lundquist, J. K., Barbieri, L., Kral, S. T., Jensen, A. A., Dixon, C., Borenstein, S., Hesselius, D., Human, K., Hall, P., Argrow, B., Thornberry, T., Wright, R., and Kelly, J. T.: Development of Community, Capabilities, and Understanding through Unmanned Aircraft-Based Atmospheric Research: The LAPSE-RATE Campaign, Bulletin of the American Meteorological Society, 101, E684–E699, https://doi.org/10.1175/BAMS-D-19-0050.1, 2020.

de Haan, S., de Jong, P. M. A., and van der Meulen, J.: Characterizing and Correcting the Warm Bias Observed in Aircraft Meteorological Data Relay (AMDAR) Temperature Observations, Atmospheric Measurement Techniques, 15, 811–818, https://doi.org/10.5194/amt-15-811-2022, 2022.

Dirksen, R. J., Sommer, M., Immler, F. J., Hurst, D. F., Kivi, R., and Vömel, H.: Reference Quality Upper-Air Measurements: GRUAN Data Processing for the Vaisala RS92 Radiosonde, Atmospheric Measurement Techniques, 7, 4463–4490, https://doi.org/10.5194/amt-7-4463-2014, 2014.

Dirksen, R. J., Bodeker, G. E., Thorne, P. W., Merlone, A., Reale, T., Wang, J., Hurst, D. F., Demoz, B. B., Gardiner, T. D., Ingleby, B., Sommer, M., von Rohden, C., and Leblanc, T.: Managing the Transition from Vaisala RS92 to RS41 Radiosondes within the Global Climate Observing System Reference Upper-Air Network (GRUAN): A Progress Report, Geoscientific Instrumentation, Methods and Data Systems, 9, 337–355, https://doi.org/10.5194/gi-9-337-2020, 2020.

Dupont, J.-C., Haeffelin, M., Badosa, J., Clain, G., Raux, C., and Vignelles, D.: Characterization and Corrections of Relative Humidity Measurement from Meteomodem M10 Radiosondes at Midlatitude Stations, Journal of Atmospheric and Oceanic Technology, 37, 857–871, https://doi.org/10.1175/JTECH-D-18-0205.1, 2020.

EASA: Easy Access Rules for Unmanned Aircraft Systems (Regulation (EU) 2019/947 and Regulation (EU) 2019/945), https://www.easa.europa.eu/document-library/easy-access-rules/easy-access-rules-unmanned-aircraft-systems-regulation-eu, 2022.

Elston, J., Argrow, B., Stachura, M., Weibel, D., Lawrence, D., and Pope, D.: Overview of Small Fixed-Wing Unmanned Aircraft for Meteorological Sampling, Journal of Atmospheric and Oceanic Technology, 32, 97–115, https://doi.org/10.1175/JTECH-D-13-00236.1, 2015.

Elston, J. S., Roadman, J., Stachura, M., Argrow, B., Houston, A., and Frew, E.: The Tempest Unmanned Aircraft System for in Situ Observations of Tornadic Supercells: Design and VORTEX2 Flight Results, Journal of Field Robotics, 28, 461–483, https://doi.org/10.1002/rob.20394, 2011.

Evtushevsky, O. M., Grytsai, A. V., Klekociuk, A. R., and Milinevsky, G. P.: Total Ozone and Tropopause Zonal Asymmetry during the Antarctic Spring, Journal of Geophysical Research: Atmospheres, 113, https://doi.org/10.1029/2008JD009881, 2008.

Eyre, J.: An Introduction to GPS Radio Occultation and Its Use in Numerical Weather Prediction., in: ECMWF GRAS SAF Workshop on Applications of GPS Radio Occultation Measurements, 16 - 18 June 2008, pp. 1–10, ECMWF, Shinfield Park, Reading, 2008.

Faccani, C., Rabier, F., Fourrié, N., Agusti-Panareda, A., Karbou, F., Moll, P., Lafore, J.-P., Nuret, M., Hdidou, F., and Bock, O.: The Impacts of AMMA Radiosonde Data on the French Global Assimilation and Forecast System, Weather and Forecasting, 24, 1268–1286, https://doi.org/10.1175/2009WAF2222237.1, 2009.

Fiedler, F. and Panofsky, H. A.: Atmospheric Scales and Spectral Gaps, Bulletin of the American Meteorological Society, 51, 1114–1120, https://doi.org/10.1175/1520-0477(1970)051<1114:ASASG>2.0.CO;2, 1970.

Flagg, D. D., Doyle, J. D., Holt, T. R., Tyndall, D. P., Amerault, C. M., Geiszler, D., Haack, T., Moskaitis, J. R., Nachamkin, J., and Eleuterio, D. P.: On the Impact of Unmanned Aerial System Observations on Numerical Weather Prediction in the Coastal Zone, Monthly Weather Review, 146, 599–622, https://doi.org/10.1175/MWR-D-17-0028.1, 2018.

Fleming, R. J.: The Use of Commercial Aircraft as Platforms for Environmental Measurements, Bulletin of the American Meteorological Society, 77, 2229–2242, https://doi.org/10.1175/1520-0477(1996)077<2229:TUOCAA>2.0.CO;2, 1996.

Fujiwara, M., Shiotani, M., Hasebe, F., Vömel, H., Oltmans, S. J., Ruppert, P. W., Horinouchi, T., and Tsuda, T.: Performance of the Meteolabor "Snow White" Chilled-Mirror Hygrometer in the Tropical Troposphere: Comparisons with the Vaisala RS80 A/H-Humicap Sensors, Journal of Atmospheric and Oceanic Technology, 20, 1534–1542, https://doi.org/10.1175/1520-0426(2003)020<1534:POTMSW>2.0.CO;2, 2003.

Geerts, B., Raymond, D. J., Grubišić, V., Davis, C. A., Barth, M. C., Detwiler, A., Klein, P. M., Lee, W.-C., Markowski, P. M., Mullendore, G. L., and Moore, J. A.: Recommendations for In Situ and Remote Sensing Capabilities in Atmospheric Convection and Turbulence, Bulletin of the American Meteorological Society, 99, 2463–2470, https://doi.org/10.1175/BAMS-D-17-0310.1, 2018.

Gelaro, R. and Zhu, Y.: Examination of Observation Impacts Derived from Observing System Experiments (OSEs) and Adjoint Models, Tellus A: Dynamic Meteorology and Oceanography, 61, 179–193, https://doi.org/10.1111/j.1600-0870.2008.00388.x, 2009.

Gettelman, A., Hoor, P., Pan, L. L., Randel, W. J., Hegglin, M. I., and Birner, T.: The Extratropical Upper Troposphere and Lower Stratosphere, Reviews of Geophysics, 49, https://doi.org/10.1029/2011RG000355, 2011.

Goldberg, M., Ohring, G., Butler, J., Cao, C., Datla, R., Doelling, D., Gärtner, V., Hewison, T., Iacovazzi, B., Kim, D., Kurino, T., Lafeuille, J., Minnis, P., Renaut, D., Schmetz, J., Tobin, D., Wang, L., Weng, F., Wu, X., Yu, F., Zhang, P., and Zhu, T.: The Global Space-Based Inter-Calibration System, Bulletin of the American Meteorological Society, 92, 467–475, https://doi.org/10.1175/2010BAMS2967.1, 2011.

Hacker, J., Draper, C., and Madaus, L.: Challenges and Opportunities for Data Assimilation in Mountainous Environments, Atmosphere, 9, 127, https://doi.org/10.3390/atmos9040127, 2018.

Hann, R.: Atmospheric Ice Accretions, Aerodynamic Icing Penalties, and Ice Protection Systems on Unmanned Aerial Vehicles, NTNU, https://ntnuopen.ntnu.no/ntnu-xmlui/handle/11250/2657638, 2020.

Hann, R., Enache, A., Nielsen, M. C., Stovner, B. N., van Beeck, J., Johansen, T. A., and Borup, K. T.: Experimental Heat Loads for Electrothermal Anti-Icing and De-Icing on UAVs, Aerospace, 8, 83, https://doi.org/10.3390/aerospace8030083, 2021.

Hersbach, H., Bell, B., Berrisford, P., Biavati, G., Horányi, A., Muñoz Sabater, J., Nicolas, J., Peubey, C., Radu, R., Rozum, I., Schepers, D., Simmons, A., Soci, C., Dee, D., and Thépaut, J.-N.: ERA5 Hourly Data on Single Levels from 1959 to Present, Copernicus Climate Change Service (C3S) Climate Data Store (CDS), https://doi.org/10.24381/cds.adbb2d47, 2018.

Hersbach, H., Bell, B., Berrisford, P., Hirahara, S., Horányi, A., Muñoz-Sabater, J., Nicolas, J., Peubey, C., Radu, R., Schepers, D., Simmons, A., Soci, C., Abdalla, S., Abellan, X., Balsamo, G., Bechtold, P., Biavati, G., Bidlot, J., Bonavita, M., Chiara, G., Dahlgren, P., Dee, D., Diamantakis, M., Dragani, R., Flemming, J., Forbes, R., Fuentes, M., Geer, A., Haimberger, L., Healy, S., Hogan, R. J., Hólm, E., Janisková, M., Keeley, S., Laloyaux, P., Lopez, P., Lupu, C., Radnoti, G., Rosnay, P., Rozum, I., Vamborg, F., Villaume, S., and Thépaut, J.-N.: The ERA5 Global Reanalysis, Q.J.R. Meteorol. Soc., 146, 1999–2049, https://doi.org/10.1002/qj.3803, 2020.

Hock, T. F. and Franklin, J. L.: The NCAR GPS Dropwindsonde, Bulletin of the American Meteorological Society, 80, 407–420, https://www.jstor.org/stable/26214911, 1999.

Holton, J. R., Haynes, P. H., McIntyre, M. E., Douglass, A. R., Rood, R. B., and Pfister, L.: Stratosphere-Troposphere Exchange, Reviews of Geophysics, 33, 403–439, https://doi.org/10.1029/95RG02097, 1995.

Houston, A. L., PytlikZillig, L. M., and Walther, J. C.: National Weather Service Data Needs for Short-Term Forecasts and the Role of Unmanned Aircraft in Filling the Gap: Results from a Nationwide Survey, Bulletin of the American Meteorological Society, 102, E2106–E2120, https://doi.org/10.1175/BAMS-D-20-0183.1, 2021.

Huang, X., Tepylo, N., Pommier-Budinger, V., Budinger, M., Bonaccurso, E., Villedieu, P., and Bennani, L.: A Survey of Icephobic Coatings and Their Potential Use in a Hybrid Coating/Active Ice Protection System for Aerospace Applications, Progress in Aerospace Sciences, 105, https://doi.org/10.1016/j.paerosci.2019.01.002, 2019.

Ingleby, B. and Edwards, D.: Changes to Radiosonde Reports and Their Processing for Numerical Weather Prediction, Atmospheric Science Letters, 16, 44–49, https://doi.org/10.1002/asl2.518, 2015.

Ingleby, B., Pauley, P., Kats, A., Ator, J., Keyser, D., Doerenbecher, A., Fucile, E., Hasegawa, J., Toyoda, E., Kleinert, T., Qu, W., James, J. S., Tennant, W., and Weedon, R.: Progress toward High-Resolution, Real-Time Radiosonde Reports, Bulletin of the American Meteorological Society, 97, 2149–2161, https://doi.org/10.1175/BAMS-D-15-00169.1, 2016a.

Ingleby, B., Rodwell, M., and Isaksen, L.: Global Radiosonde Network under Pressure, Tech. Rep. 149, ECMWF, https://doi.org/10.21957/cblxtg, 2016b.

Ingleby, B., Isaksen, L., Kral, T., and Kral, T.: Evaluation and Impact of Aircraft Humidity Data in ECMWF's NWP System, https://doi.org/10.21957/4e825dtiy, 2020.

Ingleby, B., Candy, B., Eyre, J., Haiden, T., Hill, C., Isaksen, L., Kleist, D., Smith, F., Steinle, P., Taylor, S., Tennant, W., and Tingwell, C.: The Impact of COVID-19 on Weather Forecasts: A Balanced View, Geophysical Research Letters, 48, e2020GL090 699, https://doi.org/10.1029/2020GL090699, 2021.

Ingleby, B., Motl, M., Marlton, G., Edwards, D., Sommer, M., von Rohden, C., Vömel, H., and Jauhiainen, H.: On the Quality of RS41 Radiosonde Descent Data, Atmospheric Measurement Techniques, 15, 165–183, https://doi.org/10.5194/amt-15-165-2022, 2022.

Inoue, J. and Sato, K.: Toward Sustainable Meteorological Profiling in Polar Regions: Case Studies Using an Inexpensive UAS on Measuring Lower Boundary Layers with Quality of Radiosondes, Environmental Research, 205, 112 468, https://doi.org/10.1016/j.envres.2021.112468, 2022.

Jacob, J. D., Chilson, P. B., Houston, A. L., and Smith, S. W.: Considerations for Atmospheric Measurements with Small Unmanned Aircraft Systems, Atmosphere, 9, 252, https://doi.org/10.3390/atmos9070252, 2018.

Jeck, R. K.: Icing Design Envelopes (14 CFR Parts 25 and 29, Appenddix C) Converted to a Distance-Based Format, Tech. rep., FEDERAL AVIATION ADMINISTRATION TECHNICAL CENTER ATLANTIC CITY NJ, 2002.

Jensen, A. A., Pinto, J. O., Bailey, S. C., Sobash, R. A., de Boer, G., Houston, A. L., Chilson, P. B., Bell, T., Romine, G., Smith, S. W., Lawrence, D. A., Dixon, C., Lundquist, J. K., Jacob, J. D., Elston, J., Waugh, S., and Steiner, M.: Assimilation of a Coordinated Fleet of Uncrewed Aircraft System Observations in Complex Terrain: EnKF System Design and Preliminary Assessment, Monthly Weather Review, 149, https://doi.org/10.1175/mwr-d-20-0359.1, 2021.

Jensen, A. A., Pinto, J. O., Bailey, S. C. C., Sobash, R. A., Romine, G., de Boer, G., Houston, A. L., Smith, S. W., Lawrence, D. A., Dixon, C., Lundquist, J. K., Jacob, J. D., Elston, J., Waugh, S., Brus, D., and Steiner, M.: Assimilation of a Coordinated Fleet of Uncrewed Aircraft System Observations in Complex Terrain: Observing System Experiments, Monthly Weather Review, 150, 2737–2763, https://doi.org/10.1175/MWR-D-22-0090.1, 2022.

Jonassen, M. O., Ólafsson, H., Ágústsson, H., Rögnvaldsson, Ó., and Reuder, J.: Improving High-Resolution Numerical Weather Simulations by Assimilating Data from an Unmanned Aerial System, Monthly Weather Review, 140, 3734–3756, https://doi.org/10.1175/MWR-D-11-00344.1, 2012.

Joyce, K. E., Anderson, K., and Bartolo, R. E.: Of Course We Fly Unmanned—We're Women!, Drones, 5, 21, https://doi.org/10.3390/drones5010021, 2021.

Kalinka, F., Roloff, K., Tendel, J., and Hauf, T.: The In-flight Icing Warning System ADWICE for European Airspace – Current Structure, Recent Improvements and Verification Results, Meteorologische Zeitschrift, pp. 441–455, https://doi.org/10.1127/metz/2017/0756, 2017.

Karbou, F., Aires, F., Prigent, C., and Eymard, L.: Potential of Advanced Microwave Sounding Unit-A (AMSU-A) and AMSU-B Measurements for Atmospheric Temperature and Humidity Profiling over Land, Journal of Geophysical Research: Atmospheres, 110, https://doi.org/10.1029/2004JD005318, 2005.

Kim, S.-M. and Kim, H. M.: Forecast Sensitivity Observation Impact in the 4DVAR and Hybrid-4DVAR Data Assimilation Systems, Journal of Atmospheric and Oceanic Technology, 36, 1563–1575, https://doi.org/10.1175/JTECH-D-18-0240.1, 2019.

Koch, S. E., Fengler, M., Chilson, P. B., Elmore, K. L., Argrow, B., Andra, D. L., and Lindley, T.: On the Use of Unmanned Aircraft for Sampling Mesoscale Phenomena in the Preconvective Boundary Layer, Journal of Atmospheric and Oceanic Technology, 35, 2265–2288, https://doi.org/10.1175/JTECH-D-18-0101.1, 2018.

König-Langlo, G., King, J. C., and Pettré, P.: Climatology of the Three Coastal Antarctic Stations Dumont d'Urville, Neumayer, and Halley, Journal of Geophysical Research: Atmospheres, 103, 10 935–10 946, https://doi.org/10.1029/97JD00527, 1998.

Konrad, T., Hill, M., Rowland, J., and Meyer, J. H.: A Small, Radio-Controlled Aircraft as a Platform for Meteorological Sensors, Johns Hopkins APL Tech. Dig., 10, 11–21, https://www.semanticscholar.org/paper/A-small%2C-radio-controlled-aircraft-as-a-platform-Hill-Konrad/5aaf67483ea340d40dca365d763178e8197145ea, 1970.

Kotthaus, S., Bravo-Aranda, J. A., Collaud Coen, M., Guerrero-Rascado, J. L., Costa, M. J., Cimini, D., O'Connor, E. J., Hervo, M., Alados-Arboledas, L., Jiménez-Portaz, M., Mona, L., Ruffieux, D., Illingworth, A., and Haeffelin, M.: Atmospheric Boundary Layer Height from Ground-Based Remote Sensing: A Review of Capabilities and Limitations, Atmospheric Measurement Techniques Discussions, pp. 1–88, https://doi.org/10.5194/amt-2022-14, 2022.

Kräuchi, A. and Philipona, R.: Return Glider Radiosonde for in Situ Upper-Air Research Measurements, Atmospheric Measurement Techniques, 9, 2535–2544, https://doi.org/10.5194/amt-9-2535-2016, 2016.

Kren, A. C., Cucurull, L., and Wang, H.: Impact of UAS Global Hawk Dropsonde Data on Tropical and Extratropical Cyclone Forecasts in 2016, Weather and Forecasting, 33, 1121–1141, https://doi.org/10.1175/WAF-D-18-0029.1, 2018.

Lafon, T., Fowler, J., Jiménez, J. F., and Cordoba, G. J. T.: A Viable Alternative for Conducting Cost-Effective Daily Atmospheric Soundings in Developing Countries, Bulletin of the American Meteorological Society, 95, 837–842, https://doi.org/10.1175/BAMS-D-13-00125.1, 2014.

Lampert, A., Altstädter, B., Bärfuss, K., Bretschneider, L., Sandgaard, J., Michaelis, J., Lobitz, L., Asmussen, M., Damm, E., Käthner, R., Krüger, T., Lüpkes, C., Nowak, S., Peuker, A., Rausch, T., Reiser, F., Scholtz, A., Sotomayor Zakharov, D., Gaus, D., Bansmer, S., Wehner, B., and Pätzold, F.: Unmanned Aerial Systems for Investigating the Polar Atmospheric Boundary Layer—Technical Challenges and Examples of Applications, Atmosphere, 11, 416, https://doi.org/10.3390/atmos11040416, 2020.

Langland, R. H. and Baker, N. L.: Estimation of Observation Impact Using the NRL Atmospheric Variational Data Assimilation Adjoint System, Tellus A: Dynamic Meteorology and Oceanography, 56, 189–201, https://doi.org/10.3402/tellusa.v56i3.14413, 2004.

Laursen, K. K., Jorgensen, D. P., Brasseur, G. P., Ustin, S. L., and Huning, J. R.: HIAPER: THE NEXT GENERATION NSF/NCAR RESEARCH AIRCRAFT, Bulletin of the American Meteorological Society, 87, 896–909, https://www.jstor.org/stable/26217191, 2006.

Leuenberger, D., Haefele, A., Omanovic, N., Fengler, M., Martucci, G., Calpini, B., Fuhrer, O., and Rossa, A.: Improving High-Impact Numerical Weather Prediction with Lidar and Drone Observations, Bulletin of the American Meteorological Society, 101, E1036–E1051, https://doi.org/10.1175/BAMS-D-19-0119.1, 2020.

Lindskog, M., Salonen, K., Järvinen, H., and Michelson, D. B.: Doppler Radar Wind Data Assimilation with HIRLAM 3DVAR, Monthly Weather Review, 132, 1081–1092, https://doi.org/10.1175/1520-0493(2004)132<1081:DRWDAW>2.0.CO;2, 2004.

Lorenc, A. C. and Marriott, R. T.: Forecast Sensitivity to Observations in the Met Office Global Numerical Weather Prediction System, Quarterly Journal of the Royal Meteorological Society, 140, 209–224, https://doi.org/10.1002/qj.2122, 2014.

Majewski, J.: The Dynamic Behaviour of Capacitive Humidity Sensors, Devices and Methods of Measurements, 11, 53–59, https://doi.org/10.21122/2220-9506-2020-11-1-53-59, 2020.

Miloshevich, L. M., Paukkunen, A., Vömel, H., and Oltmans, S. J.: Development and Validation of a Time-Lag Correction for Vaisala Radiosonde Humidity Measurements, Journal of Atmospheric and Oceanic Technology, 21, 1305–1327, https://doi.org/10.1175/1520-0426(2004)021<1305:DAVOAT>2.0.CO;2, 2004.

Moninger, W. R., Mamrosh, R. D., and Pauley, P. M.: Automated Meteorological Reports from Commercial Aircraft, Bulletin of the American Meteorological Society, 84, 203–216, https://doi.org/10.1175/BAMS-84-2-203, 2003.

Moninger, W. R., Benjamin, S. G., Jamison, B. D., Schlatter, T. W., Smith, T. L., and Szoke, E. J.: Evaluation of Regional Aircraft Observations Using TAMDAR, Weather and Forecasting, 25, 627–645, https://doi.org/10.1175/2009WAF2222321.1, 2010.

Nash, J., Oakley, T., Vömel, H., and Wei, L.: IOM Report, 107. WMO Intercomparison of High Quality Radiosonde Systems, WMO/TD, World Meteorological Organization, Geneva, 2011.

Ota, Y., Derber, J. C., Kalnay, E., and Miyoshi, T.: Ensemble-Based Observation Impact Estimates Using the NCEP GFS, Tellus A: Dynamic Meteorology and Oceanography, 65, 20 038, https://doi.org/10.3402/tellusa.v65i0.20038, 2013.

Palmer, R., Whelan, D., Bodine, D., Kirstetter, P., Kumjian, M., Metcalf, J., Yeary, M., Yu, T.-Y., Rao, R., Cho, J., Draper, D., Durden, S., English, S., Kollias, P., Kosiba, K., Wada, M., Wurman, J., Blackwell, W., Bluestein, H., Collis, S., Gerth, J., Tuttle, A., Wang, X., and Zrnić, D.: The Need for Spectrum and the Impact on Weather Observations, Bulletin of the American Meteorological Society, 102, E1402–E1407, https://doi.org/10.1175/BAMS-D-21-0009.1, 2021.

Pätzold, F.: Windmessung mittels Segelflugzeug, Forschungsbericht 2018-04, Niedersächsisches Forschungszentrum für Luftfahrt, Braunschweig, Germany, https://doi.org/10.24355/dbbs.084-201805221102-1, 2018.

Pena-Ortiz, C., Gallego, D., Ribera, P., Ordonez, P., and Alvarez-Castro, M. D. C.: Observed Trends in the Global Jet Stream Characteristics during the Second Half of the 20th Century, Journal of Geophysical Research: Atmospheres, 118, 2702–2713, https://doi.org/10.1002/jgrd.50305, 2013.

Petersen, R. A.: On the Impact and Benefits of AMDAR Observations in Operational Forecasting—Part I: A Review of the Impact of Automated Aircraft Wind and Temperature Reports, Bulletin of the American Meteorological Society, 97, 585–602, https://doi.org/10.1175/BAMS-D-14-00055.1, 2016.

Petersen, R. A., Cronce, L., Mamrosh, R., and Baker, R.: A Report to the World Meteorological Organization on the Impact and Benefits of AMDAR Temperature, Wind and Moisture Observations in Operational Weather Forecasting, Tech. rep., University of Wisconsin-Madison, Cooperative Institute for Meteorological Satellite Studies, Space Science and Engineering center, https://search.library.wisc.edu/catalog/9911154629902121, 2015.

Petersen, R. A., Cronce, L., Mamrosh, R., Baker, R., and Pauley, P.: On the Impact and Future Benefits of AMDAR Observations in Operational Forecasting: Part II: Water Vapor Observations, Bulletin of the American Meteorological Society, 97, 2117–2133, https://doi.org/10.1175/BAMS-D-14-00211.1, 2016.

Pinto, J. O., O'Sullivan, D., Taylor, S., Elston, J., Baker, C. B., Hotz, D., Marshall, C., Jacob, J., Barfuss, K., Piguet, B., Roberts, G., Omanovic, N., Fengler, M., Jensen, A. A., Steiner, M., and Houston, A. L.: The Status and Future of Small Uncrewed Aircraft Systems (UAS) in Operational Meteorology, Bulletin of the American Meteorological Society, 102, E2121–E2136, https://doi.org/10.1175/BAMS-D-20-0138.1, 2021.

Rabier, F., Bouchard, A., Brun, E., Doerenbecher, A., Guedj, S., Guidard, V., Karbou, F., Peuch, V.-H., Amraoui, L. E., Puech, D., Genthon, C., Picard, G., Town, M., Hertzog, A., Vial, F., Cocquerez, P., Cohn, S. A., Hock, T., Fox, J., Cole, H., Parsons, D., Powers, J., Romberg, K., VanAndel, J., Deshler, T., Mercer, J., Haase, J. S., Avallone, L., Kalnajs, L., Mechoso, C. R., Tangborn, A., Pellegrini, A., Frenot, Y., Thépaut, J.-N., McNally, A., Balsamo, G., and Steinle, P.: The Concordiasi Project in Antarctica, Bulletin of the American Meteorological Society, 91, 69–86, https://doi.org/10.1175/2009BAMS2764.1, 2010.

Ralph, F. M., Cannon, F., Tallapragada, V., Davis, C. A., Doyle, J. D., Pappenberger, F., Subramanian, A., Wilson, A. M., Lavers, D. A., Reynolds, C. A., Haase, J. S., Centurioni, L., Ingleby, B., Rutz, J. J., Cordeira, J. M., Zheng, M., Hecht, C., Kawzenuk, B., and Monache, L. D.: West Coast Forecast Challenges and Development of Atmospheric River Reconnaissance, Bulletin of the American Meteorological Society, 101, E1357–E1377, https://doi.org/10.1175/BAMS-D-19-0183.1, 2020.

Rautenberg, A., Graf, M. S., Wildmann, N., Platis, A., and Bange, J.: Reviewing Wind Measurement Approaches for Fixed-Wing Unmanned Aircraft, Atmosphere, 9, 422, https://doi.org/10.3390/atmos9110422, 2018.

Redelsperger, J.-L., Thorncroft, C. D., Diedhiou, A., Lebel, T., Parker, D. J., and Polcher, J.: African Monsoon Multidisciplinary Analysis: An International Research Project and Field Campaign, Bulletin of the American Meteorological Society, 87, 1739–1746, https://doi.org/10.1175/BAMS-87-12-1739, 2006.

Reineman, B. D., Lenain, L., and Melville, W. K.: The Use of Ship-Launched Fixed-Wing UAVs for Measuring the Marine Atmospheric Boundary Layer and Ocean Surface Processes, Journal of Atmospheric and Oceanic Technology, 33, 2029–2052, https://doi.org/10.1175/JTECH-D-15-0019.1, 2016.

Rennie, M. P., Isaksen, L., Weiler, F., de Kloe, J., Kanitz, T., and Reitebuch, O.: The Impact of Aeolus Wind Retrievals on ECMWF Global Weather Forecasts, Quarterly Journal of the Royal Meteorological Society, 147, 3555–3586, https://doi.org/10.1002/qj.4142, 2021.

Riishojgaard, D. L. P.: Wind Measurements in the WMO Global Observing System, ESA Workshop, p. 31, 2015.

Runge, H., Rack, W., Alba, R.-L., and Hepperle, M.: A Solar-Powered HALE-UAV for Arctic Research, in: CEAS Conference 2007, pp. 1–6, Berlin, https://elib.dlr.de/51266/, 2007.

Schindler, M., Weissmann, M., Schäfler, A., and Radnoti, G.: The Impact of Dropsonde and Extra Radiosonde Observations during NAWDEX in Autumn 2016, Monthly Weather Review, 148, 809–824, https://doi.org/10.1175/MWR-D-19-0126.1, 2020.

Schuyler, T. J., Gohari, S. M. I., Pundsack, G., Berchoff, D., and Guzman, M. I.: Using a Balloon-Launched Unmanned Glider to Validate Real-Time WRF Modeling, Sensors, 19, 1914, https://doi.org/10.3390/s19081914, 2019.

Secretariat of the Antarctic Treaty: Compilation of Key Documents of the Antarctic Treaty, Secretariat of the Antarctic Treaty, Buenos Aires, fourth edition edn., https://documents.ats.aq/atcm42/ww/ATCM42_ww011_e.pdf, 2019.

Sørensen, K. L., Borup, K. T., Hann, R., and Hansbø, M.: UAV Atmospheric Icing Limitations, Climate Report Sor Norway and Surrounding Regions, Tech. rep., UBIQ Aerospace, 2021.

Steiner, A. K., Kirchengast, G., Foelsche, U., Kornblueh, L., Manzini, E., and Bengtsson, L.: GNSS Occultation Sounding for Climate Monitoring, Physics and Chemistry of the Earth, Part A: Solid Earth and Geodesy, 26, 113–124, https://doi.org/10.1016/S1464-1895(01)00034-5, 2001.

Stickney, T. M., Shedlov, M. W., and Thompson, D. I.: GOODRICH TOTAL TEMPERATURE SENSORS, Tech. rep., Goodrich, 1994.

Sun, Q., Vihma, T., Jonassen, M. O., and Zhang, Z.: Impact of Assimilation of Radiosonde and UAV Observations from the Southern Ocean in the Polar WRF Model, Adv. Atmos. Sci., 37, 441–454, https://doi.org/10.1007/s00376-020-9213-8, 2020.

Tafferner, A., Hauf, T., Leifeld, C., Hafner, T., Leykauf, H., and Voigt, U.: ADWICE: Advanced Diagnosis and Warning System for Aircraft Icing Environments, Weather and Forecasting, 18, 184–203, https://doi.org/10.1175/1520-0434(2003)018<0184:AADAWS>2.0.CO;2, 2003.

Thépaut, J.-N. and Andersson, E.: The Global Observing System, in: Data Assimilation: Making Sense of Observations, edited by Lahoz, W., Khattatov, B., and Menard, R., pp. 263–281, Springer, Berlin, Heidelberg, https://doi.org/10.1007/978-3-540-74703-1_10, 2010.

VAISALA: Response Time in Humidity Measurement, TECHNICAL NOTE B211803EN-B, VAISALA, https://www.vaisala.com/sites/default/files/documents/Response-time-in-humidity-measurement-Technical-Note-B211803EN.pdf, 2021.

Vinnichenko, N. K.: The Kinetic Energy Spectrum in the Free Atmosphere—1 Second to 5 Years, Tellus, 22, 158–166, https://doi.org/10.3402/tellusa.v22i2.10210, 1970.

Vömel, H., Argrow, B. M., Axisa, D., Chilson, P., Ellis, S., Fladeland, M., Frew, E. W., Jacob, J., Lord, M., Moore, J., Oncley, S., Roberts, G., Schoenung, S., and Wolff, C.: The NCAR/EOL Community Workshop on Unmanned Aircraft Systems for Atmospheric Research - Final Report, none, https://doi.org/10.5065/D6X9292S, 2018.

Wagner, T. J. and Petersen, R. A.: On the Performance of Airborne Meteorological Observations against Other In Situ Measurements, Journal of Atmospheric and Oceanic Technology, 38, 1217–1230, https://doi.org/10.1175/JTECH-D-20-0182.1, 2021.

Wang, B., Zou, X., and Zhu, J.: Data Assimilation and Its Applications, Proceedings of the National Academy of Sciences, 97, 11 143–11 144, https://doi.org/10.1073/pnas.97.21.11143, 2000.

Wang, J., Hock, T., Cohn, S. A., Martin, C., Potts, N., Reale, T., Sun, B., and Tilley, F.: Unprecedented Upper-Air Dropsonde Observations over Antarctica from the 2010 Concordiasi Experiment: Validation of Satellite-Retrieved Temperature Profiles, Geophysical Research Letters, 40, 1231–1236, https://doi.org/10.1002/grl.50246, 2013.

Watts, A. C., Ambrosia, V. G., and Hinkley, E. A.: Unmanned Aircraft Systems in Remote Sensing and Scientific Research: Classification and Considerations of Use, Remote Sensing, 4, 1671–1692, https://doi.org/10.3390/rs4061671, 2012.

WMO: AMDAR Reference Manual: Aircraft Meteorological Data Relay, no. 958 in WMO, Secretariat of the World Meteorological Organization, Geneva, 2003.

WMO: Guide to the Global Observing System, WMO, World Meteorological Organization, Geneva, 2010 edition updated in 2017 edn., 2010.

WMO: Global Observing System, https://public.wmo.int/en/programmes/global-observing-system, 2015a.

WMO: OSCAR - Observing Systems Capability Analysis and Review Tool, WMO, Geneva, 2015b.

WMO: Guide to Instruments and Methods of Observation, no. 8 in WMO, WMO, Geneva, 2018 edition edn., 2018.

WMO: The Gaps in the Global Basic Observing Network (GBON), Tech. rep., WMO Systematic Observations Financing Facility, https://public.wmo.int/en/resources/library/gaps-global-basic-observing-network-gbon, 2020.

WMO: WMO UAS Demonstration Campaign Description | World Meteorological Organization, https://community.wmo.int/uas-demonstration/description, 2022.

Wyngaard, J., Barbieri, L., Thomer, A., Adams, J., Sullivan, D., Crosby, C., Parr, C., Klump, J., Raj Shrestha, S., and Bell, T.: Emergent Challenges for Science sUAS Data Management: Fairness through Community Engagement and Best Practices Development, Remote Sensing, 11, 1797, https://doi.org/10.3390/rs11151797, 2019.

Zheng, M., Delle Monache, L., Cornuelle, B. D., Ralph, F. M., Tallapragada, V. S., Subramanian, A., Haase, J. S., Zhang, Z., Wu, X., Murphy, M. J., Higgins, T. B., and DeHaan, L.: Improved Forecast Skill Through the Assimilation of Dropsonde Observations From the Atmospheric River Reconnaissance Program, Journal of Geophysical Research: Atmospheres, 126, e2021JD034 967, https://doi.org/10.1029/2021JD034967, 2021.